

Synthesis and SERS: Reproducible Nanostar Plasmons and a Study of Optical  
Enhancement

by

Jacob D. Ramsey

A THESIS

submitted to

Oregon State University

University Honors College

in partial fulfillment of  
the requirements for the  
degree of

Honors Baccalaureate of Science in Chemistry  
(Honors Scholar)

Presented June 1, 2016  
Commencement June 2016



## AN ABSTRACT OF THE THESIS OF

Jacob D. Ramsey for the degree of Honors Baccalaureate of Science in Chemistry presented on June 1, 2016. Title: Synthesis and SERS: Reproducible Nanostar Plasmons and a Study of Optical Enhancement.

Abstract approved:

---

Sean M. Burrows

Gold nanostars are a relative newcomer to the nanoparticle scene, and their unique properties make them very desirable for spectroscopic applications. These nanoparticles, with their sharp tips, create electric field enhancements that interact with light in an advantageous way. This Thesis outlines our in-depth study of gold nanostar synthesis, the factors that influence it, and a novel technique for creating these particles with a reproducible plasmon band. This plasmon band gives rise to the Surface Enhanced Raman Scattering (SERS) and Metal Enhanced Fluorescence (MEF) effects. Our goal is to design innovative new biosensors using these phenomena to increase the number of microRNA's we can detect, increase sensitivity, and develop new tools for medical diagnostics. This Thesis covers our initial endeavors into these fields and characterizes how our gold nanostars enhance signals and the factors influencing their optical response. We demonstrate the capability to obtain MEF and obtain highly sensitive SERS measurements, which are the first steps in utilizing these technologies for future biosensors.

Key Words: Gold Nanostar, Plasmon, Surface Enhanced Raman Scattering (SERS), Reproducibility

Corresponding e-mail address: [ramseyja@oregonstate.edu](mailto:ramseyja@oregonstate.edu)

©Copyright by Jacob D. Ramsey  
June 1, 2016  
All Rights Reserved

Synthesis and SERS: Reproducible Nanostar Plasmons and a Study of Optical  
Enhancement

by

Jacob D. Ramsey

A THESIS

submitted to

Oregon State University

University Honors College

in partial fulfillment of  
the requirements for the  
degree of

Honors Baccalaureate of Science in Chemistry  
(Honors Scholar)

Presented June 1, 2016  
Commencement June 2016

Honors Baccalaureate of Science in Chemistry project of Jacob D. Ramsey presented on June 1, 2016.

APPROVED:

---

Sean M. Burrows , Mentor, representing The Department of Chemistry

---

Chong Fang, Committee Member, representing The Department of Chemistry

---

Lixia Zhou, Committee Member, representing The Department of Chemistry

---

Toni Doolen, Dean, University Honors College

I understand that my project will become part of the permanent collection of Oregon State University, University Honors College. My signature below authorizes release of my project to any reader upon request.

---

Jacob D. Ramsey, Author

## Table of Contents

Chapter 1- Achieving Plasmon Reproducibility in Surfactant Free Gold Nanostar  
Synthesis

Chapter 2-Experiments in Metal Enhanced Fluorescence: Proof of Enhancement

Chapter 3-Building a Raman Instrument

Chapter 4- Experiments in Surface Enhanced Raman Scattering: Using Plasmons to  
Enhance Signals

## Acknowledgements

I would like to thank my parents for always pushing me to do my best, and always making me believe that there is no ceiling to what I can achieve.

To Dr. Sean Burrows for always teaching me and believing in my work even when I did not. Thank you for trusting me, believing in me, supporting me, and letting me be independent with my work. You have introduced me to the world of chemistry, and I never want to leave.

Kyle Almlie, you taught me everything I needed to know to get started in this lab, and I continue to learn from you each time I step in there. Thank you for performing the laborious task of training this undergraduate who never seems to stop having questions for you.

## Chapter 1

### Achieving Plasmon Reproducibility in Surfactant Free Gold Nanostar Synthesis

This Chapter is reproduced from the paper titled “Achieving Plasmon Reproducibility in Surfactant Free Gold Nanostar Synthesis,” by Ramsey *et. al.* with permission from the New Journal of Chemistry (RSC).

## INTRODUCTION

Nanostars are nanomaterials with spikes protruding from a spherical core. The sharp spikes facilitate strong Local Surface Plasmon Resonances (LSPRs) in the red to near infrared (NIR) spectral region. The strong LSPRs create a local electric field enhancement on the tip and between the sharp spikes on the individual stars as well as between the spikes of adjacent stars.<sup>1-5</sup> These attributes make them excellent tools in the emerging field of plasmonics.<sup>6-8</sup> The LSPR and near electric field enhancement result from the oscillation of conduction electrons interacting with light at the surface of the nanostar.<sup>6</sup> The peak plasmon resonance wavelength, referred to as  $\lambda_{\max}$ , and electric field enhancement are heavily dependent on the size and shape of the particles and are often proportional to the length and aspect ratio of the spikes.<sup>1,7-10</sup> The spike length and aspect ratio influence the observed red shift of the nanostars plasmon away from the 520 nm peak of the gold nanosphere seed particles.<sup>1</sup> Additional electric field enhancement comes from the hybridization of plasmons from the spike tip and nanosphere core.<sup>9</sup> Hybridization of the plasmons from the various spike aspect ratios, as well as core and spike plasmon hybridization, give the nanostars plasmon resonance extinction spectrum a broad spectral profile. Typically, the Full Width Half Maximum of the spectrum extends over 150 nm.<sup>1,11</sup>

Biocompatible gold nanostars are of great value as their small size (30-60 nm) allows them to fit on and inside of cells.<sup>1</sup> Their unique optical properties make them excellent tools for analytical techniques and therapeutic applications, as gold nanoparticles have demonstrated reduced toxicity in human studies<sup>1,12</sup> For biological applications, a  $\lambda_{\max}$  in the NIR is particularly useful. Compared to plasmon resonances excited at shorter wavelengths, NIR excitation allows for greater tissue penetration, reduced background from autofluorescence and light scatter, and causes less photothermal heat damage to the samples.<sup>10,13</sup> Gold nanostars have many potential applications such as medical diagnostics, biosensing, gyromagnetic imaging, photonic imaging, electronics, and others.<sup>3,4,6,14,15</sup> Each application could potentially require a different  $\lambda_{\max}$ , which introduces a need for  $\lambda_{\max}$  tunability. Additionally, for nanostars to be used as a reliable tool they require reproducible signals.<sup>15-17</sup>

The optical signal response is intrinsic to the nanostars geometric structure; however, the signal is usually an ensemble average from many nanostars. While it is virtually impossible to create nanostars with homogeneous structure, the average structure and collective signal needs to be reproducible for use as a reliable nanomaterial. There are some reports on the reproducibility of Surface Enhanced Raman Scattering (SERS) signal for other types of nanoparticle geometries.<sup>18-20</sup> Often these reports were on the SERS reproducibility between a nanogap or of a single particle rather than focusing on the fundamental plasmon resonance from an ensemble of many particles. For these reasons, a synthesis technique is needed that produces nanostars with a reproducible plasmon resonance peak and spectral profile.

Many methods of nanostar synthesis exist, typically involving seed-mediated growth that begins with gold nanospheres as a substrate for growing the spikes to make star shapes.<sup>1,6,16</sup> Seedless methods also exist but are less common.<sup>21,22</sup> The nanostar growth mechanism is strongly controlled by the local dielectric environment, and any small change to this can affect the synthesis.<sup>4,23,24</sup> Another factor that heavily influences the synthesis of the nanostars is the surface roughness of the nanosphere seed particles.<sup>7,25</sup> Surfactants such as Polyvinylpyrrolidone (PVP) or Cetyl Trimethylammonium Bromide (CTAB) are often used to mediate the growth of the spikes on the nanosphere surface.<sup>11,13,21,22</sup> These surfactants and others demonstrate cytotoxicity that limits their use in biological applications.<sup>1,3,26</sup> In some cases the complete post synthesis removal of these surfactants is very difficult to achieve.<sup>1,27</sup>

Biologically compatible nanostars using weakly interacting surfactants have been studied in-depth by the Pallavicini group.<sup>27-30</sup> These surfactants have been easily replaced post synthesis with thiol containing molecules and a centrifugal wash.<sup>27,30</sup> These methods of biocompatible gold nanostar synthesis have been successful, but they require longer reaction times and extra steps to replace surfactants with other surface coatings.<sup>27,29</sup> Additionally, some of the studies note the lack of monodispersity as three distinctly different morphologies were created from their synthesis procedures.<sup>27,29</sup> Work by others with surfactant-mediated approaches, and our own experiences with surfactant-free gold nanostar synthesis, revealed that each centrifugation step had the potential for loss of nanomaterial and increased the potential for undesired

aggregation.<sup>1,14</sup> For biological applications, the relative ease of synthesis and monodispersity of the product in surfactant-free synthesis circumvents any potential issues associated with surfactant-mediated techniques.<sup>1,14,21</sup>

Dey *et al.* and others remark that there is a lack of facile and robust procedures for synthesizing biocompatible gold nanostars that are both monodisperse and have reproducible plasmon resonances.<sup>5,31,32</sup> Reproducible plasmon resonances are needed for any application. For example, if  $\lambda_{\max}$  and the plasmon band shape are not reproducible, then the Surface Enhanced Resonant Raman signal can drastically change.<sup>33</sup> Thus, a reproducible surfactant-free method for nanostar synthesis is necessary for any field, especially those working in biological applications.<sup>17,18</sup>

According to work by Yuan *et al.*, the nanostar growth in surfactant-free methods is controlled by Ascorbic Acid and Silver Nitrate ( $\text{AgNO}_3$ ) concentration.<sup>1</sup> Previous methods have controlled growth via  $\text{HAuCl}_4$  concentration.<sup>7</sup> Current understanding of this nanostar synthesis mechanism suggests that ascorbic acid reduces Au (III) to Au (0) on the gold nanosphere seed particle surface, and the  $\text{AgNO}_3$  concentration controls the anisotropic growth of the spikes.<sup>1</sup> Higher concentrations of  $\text{AgNO}_3$  increase the spike length and surface coverage, directly controlling the  $\lambda_{\max}$ .<sup>1,13</sup>

Following the surfactant-free gold nanostar synthesis of others we found it difficult to obtain reproducible plasmon band positions and profiles.<sup>1</sup> Variables such as pH and seed particle concentration have briefly been explored by Yuan *et al.*<sup>1</sup> They found that lowering the pH of the synthesis solution would lead to more red-shifted plasmon bands as would using fewer seed particles as it created larger nanostars.<sup>1</sup> The effect of temperature on nanostar  $\lambda_{\max}$  position in a surfactant mediated synthesis technique was briefly addressed by Barbosa *et al.*, but they only conducted experiments above room temperature.<sup>6</sup> Nucleation theory states that lower temperatures will decrease the activation energy and critical radius needed to initiate growth of the nanoparticles post nucleation. Additionally, the lower temperature will increase the number of stable nuclei but decrease the frequency of attachment of atoms in the liquid phase to the solid phase. These fundamental principles of nucleation provide a theoretical basis for low temperature synthesis influencing the geometric and plasmonic properties of nanostar synthesis.<sup>34</sup> To the best of our knowledge, a detailed

study on the reproducibility of surfactant-free, seed mediated gold nanostar plasmon resonance and the use of temperature, between 5 and 90 °C, to control reproducibility of the plasmon resonance has not been investigated.

Here we investigate the gold nanostar surfactant-free synthesis conditions that generate reproducible plasmon bands. Specifically, we were interested in the geometric shape, plasmon position, and plasmon reproducibility. Several synthesis conditions were evaluated in an attempt to achieve nanostars with a reproducible plasmon resonance in the NIR region. Here we explore pH, salt concentration, seed particle concentration, reaction time, and temperature as we follow the surfactant-free synthesis technique of Yuan *et al.*<sup>1</sup> Only the reaction temperature demonstrated sufficient control over the synthesis to give nanostars with reproducible plasmon resonances. The temperature controlled synthesis method has been developed along with adjustable AgNO<sub>3</sub> concentration as a significant step towards obtaining surfactant-free, biocompatible nanostars with plasmon resonances that are both tunable and reproducible. UV/Vis data were analyzed for statistical differences in the standard deviation of plasmon band positions and bandwidths. TEM images were analyzed to learn about the geometric shape of the nanostars at different synthesis temperatures.

## **EXPERIMENTAL**

### ***Materials and Instrumentation***

Gold Chloride (HAuCl<sub>4</sub>) Hydrate (Tetrachloroauric Acid) (99.999 %) was purchased from Sigma Aldrich, L-Ascorbic Acid (99.0 %), Hydrochloric acid (ACS grade), and Sodium Chloride (ACS grade) were purchased from Macron Chemical, Sodium Nitrate (ACS grade) and Nitric acid (ACS grade) were purchased from EMD, Sodium Citrate (99 %) was purchased from Acros, and Silver Nitrate (99.9 %) was purchased from Alfa Aesar. All reagents were used as received. All solutions were prepared using house de-ionized (DI) water. Gold seed particles were synthesized according to the procedures described by Yuan *et al.*<sup>1</sup> Briefly, 15 mL of a 1% trisodium citrate solution was added to 100 mL of boiling 1 mM HAuCl<sub>4</sub> with vigorous stirring. Small additions of DI water added to this solution kept the volume constant over the 15-minute reaction period. After cooling, the solution was filtered through a 0.22 μm

nitrocellulose membrane (Corning, product # 430756). The gold seed solution was protected from light and kept at 4 °C for long-term storage.

Nanostars and seed solutions were characterized with UV/Vis spectrophotometry, Nanosight, and Transmission Electron Microscopy (TEM). A UV 1800 UV/Vis Shimadzu Spectrophotometer (Shimadzu, Kyoto, Japan) was used to obtain the nanostar spectral profiles. The following settings were used on the UV/Vis spectrophotometer: pitch-2.0 nm, Scan Speed-fast, Absorbance-0.000-2.000. A cell with a 1 cm path length was used for all UV/Vis measurements. Images of nanostars were obtained using a FEI Titan 80-200 TEM/STEM (FEI, Hillsboro, OR, USA, 80 kV or 200 kV). Concentration and average size information was obtained using a Nanosight NS 500 (Nanosight Ltd, Salisbury, UK).

### ***Synthesis of Gold Nanostars at Different Temperatures***

Biocompatible gold nanostars were synthesized using a modified surfactant-free procedure based on the techniques developed by Yuan *et al.*<sup>1</sup> Briefly, we doubled the volume of all reagents used in the synthesis in order to have enough material for characterization. 20 mL of 0.25 mM Gold Chloride was mixed with 20  $\mu$ L of 1 M HCl and 200  $\mu$ L of Gold Seed Particles (~ 12 nm) with moderate to vigorous stirring at about 800 rpm. For all reactions 100  $\mu$ L of 100 mM Ascorbic Acid and 200  $\mu$ L of a stock 3.0 mM AgNO<sub>3</sub> were added simultaneously with pipettes straight up and down as soon as possible after combining the first three reagents. For nanostars synthesized above room temperature, beakers containing gold chloride, HCl, and gold seed particles were heated to the desired temperature. For synthesis below room temperature a water-ice bath was used. Once the desired temperature was reached, AgNO<sub>3</sub> and ascorbic acid were added to initiate the reaction. For the comparison of plasmon reproducibility under different AgNO<sub>3</sub> concentrations, we used 2.0 mM (S20 nanostars) and 3.5 mM (S35 nanostars) stock AgNO<sub>3</sub> instead of 3.0 mM AgNO<sub>3</sub> (S30 nanostars). The S20 and S35 nanostars also used 200  $\mu$ L of their respective stock solutions.

Unless otherwise stated, the nanostar reaction was allowed to proceed for 30 seconds. The reaction was quenched by centrifugation at 2000 rcf (relative centrifugal force) for 15 minutes. After centrifugation, the pellet was not completely solid and loss

of material was a concern. To prevent loss of nanostar material, the supernatant was removed until only 2 mL remained. To disrupt aggregated particles, the samples were then sonicated for 8 minutes before filtering (0.22  $\mu\text{m}$  nitrocellulose membrane). Filtering helps remove large or aggregated particles. The process of centrifugation was repeated twice after filtering. For these final centrifugation steps the supernatant was completely removed after each centrifugation, and the material was re-dispersed in 1 mL of DI water. Immediately following the final centrifugation, UV/Vis spectra were obtained for the samples.

Throughout the course of these experiments we found that multiple centrifugations reduced the yield and can lead to undesired aggregation. For optimal results we recommend only one additional centrifugation after quenching. After centrifugation the gold nanostars were condensed in a pellet at the bottom of the tube. If stored in this way the nanostars will aggregate and be rendered useless. It is essential to allow the nanostars to stay in pellet form for a minimal time period to prevent aggregation at all steps. Samples were resuspended in DI water after centrifugation and kept at 4  $^{\circ}\text{C}$  for long-term storage.

All glassware and stir bars were washed with aqua regia (3:1,  $\text{HCl}:\text{HNO}_3$ ) between uses. Proper safety precautions should be followed as  $\text{HCl}$  and  $\text{HNO}_3$  are strong acids and  $\text{HNO}_3$  is a strong oxidizing agent. Sodium Bicarbonate or alternative neutralizer should be used prior to disposal of acid waste.

### ***Measurement of Nanostar Dimensions***

The core diameter, tip-to-tip distance, spike length, and aspect ratio of nanostars were measured at 5, 25, and 40  $^{\circ}\text{C}$  using their respective TEM images in ImageJ software. At each temperature, five nanostars were analyzed. The core diameter and tip-to-tip distance were measured twice for each star. Four spikes on each nanostar were selected at random and measured as the length from the tip of the spike to its base defined by the edge of the core. One criterion for selection of a nanostar for measurement was that it could be visually well resolved from other nanostars. This limited the sample size we could measure. The aspect ratio of the spikes was

determined using the length and width of the spikes. Because the width of the spikes changes along the length, we used the base width of the spikes.

### ***Procedures for Determination of Au (III) to Au (0) Conversion Yield***

To determine the conversion yield of Au (III) to Au (0) during synthesis of the nanostars at 5 and 25 °C, the UV/Vis peak of the gold chloride was monitored at 306 nm. The UV/Vis of just the gold chloride solution was taken before addition of gold seed solution, HCl, ascorbic acid, and AgNO<sub>3</sub>. For each temperature, three replicate 20 mL aliquots of gold chloride were mixed with HCl, ascorbic acid, and AgNO<sub>3</sub> for 30 seconds (as described above). To quench the synthesis, each replicate was separated into two 10 mL aliquots using 15 mL centrifuge tubes and centrifuged as described above. Immediately after the first centrifugation, the supernatant was sampled by removal of 8 mL from each vial and recombined (this was done for each replicate). The supernatant was then centrifuged again to make sure any nanostars carried over were pushed to bottom of centrifuge tube. Finally, UV/Vis analysis of the supernatant was used to determine the amount of gold chloride left over after the synthesis.

### ***Solution Preparation for Aggregation Potential Study***

Aggregation potential was determined from nanostars made at 5 and 25 °C by two of the authors, Jacob Ramsey (JR) and Lixia Zhou (LZ). Two authors were used to demonstrate trends between two different people making the nanostars. The concentrations of the nanostars made at each temperature by each author were determined with the Nanosight. After determining the concentration, each nanostar solution was brought to a concentration of  $5 \times 10^{10}$  nanostars/mL. These solutions were then used to prepare solutions containing a final concentration of  $1 \times 10^{10}$  nanostars/mL and 0, 15, 30, 75, and 150 mM NaCl.

## **RESULTS AND DISCUSSION**

### ***Reaction Conditions Influencing Gold Nanostar Synthesis***

In general, synthesis of nanoparticles is difficult to reproduce and is heavily influenced by the local chemical and physical environment. Utilizing a surfactant-free

nanostar synthesis technique, we attempted to obtain a reproducible  $\lambda_{\max}$  in the NIR region.<sup>1</sup> Many factors were explored with varying degrees of success. These factors included pH, salt concentration (ionic strength), seed particle concentration, reaction time, and temperature.

The pH, salt concentration, and seed particle concentration were only briefly explored because aggregation, lack of colloidal suspension, and lack of  $\lambda_{\max}$  reproducibility prevented further analysis (data not shown). After centrifugation, the nanostars were concentrated in a pellet at the bottom of the centrifuge vial and would usually readily resuspend into solution. However, studies in pH, salt concentration, and seed particle concentration often did not resuspend. The ionic strength of the reaction solution as described above was calculated to be 3.565 mM. We found changes in the ionic strength with NaCl and NaNO<sub>3</sub> by hundreds of micromolar or more influenced the morphology of the nanostars or caused them to aggregate. Even if the nanostars did not aggregate, the  $\lambda_{\max}$  values were not reproducible. For solutions with decreased pH and lower concentrations of seed particle that did resuspend, red shifts further into the NIR region were observed. However, these changes significantly decreased nanostar yield as most of the nanostars spontaneously aggregated and did not readily suspend in solution. Due to aggregation of a majority of the nanostars, the samples were rendered useless, and these factors were not explored further.

### ***Effect of Nanostar Synthesis Temperature on Plasmon Resonance Position and Reproducibility***

The effect of temperature on the synthesis of gold nanostars has been studied for methods using surfactants at temperatures above room temperature (25 °C).<sup>6</sup> Here we investigated the effects of temperature on surfactant-free nanostar synthesis both above and below 25 °C. The results of surfactant mediated synthesis techniques do not directly match those of the surfactant-free methods we performed and cannot be extrapolated to this study.

The effect of temperature on nanostar synthesis was investigated at 0, 5, 25, 40, 50, and 90 °C. UV/Vis spectra and Transmission Electron Microscopy (TEM) images were used to determine temperature effects on the nanostars optical properties and

physical appearance, respectively. To gauge the reproducibility of the synthesis at different temperatures the standard deviation of the  $\lambda_{\text{max}}$  position and spectral width at three quarters full maximum were used. Full width half maximum was not used because some of the nanostars absorbed and scattered light near the upper limit of the spectrophotometers wavelength range (1000 nm).

Figures 1(a) and 2 demonstrate that at 5 °C a reproducible plasmon band was observed with an average  $\lambda_{\text{max}}$  of 751 nm and a standard deviation of  $\pm 4$  nm ( $n = 4$ ,  $\sim 0.5$  %relative standard deviation, RSD). The spectral width at three quarters full maximum ranged from 164 nm to 182 nm and averaged  $174 \pm 8$  nm ( $n = 4$ ,  $\sim 5$  % RSD). Synthesis at room temperature (25 °C) gave an average  $\lambda_{\text{max}}$  of 818 nm, but varied greatly with a standard deviation of  $\pm 39$  nm ( $n = 4$ ,  $\sim 5$  % RSD) (Figures 1(b) and 2). At 25 °C the width of the spectral profile at three quarters full maximum ranged from 202 to 338 nm and averaged about  $254 \pm 60$  nm ( $n = 4$ ,  $\sim 24$  % RSD). The standard deviation of the  $\lambda_{\text{max}}$  (Figure 2) and peak width for nanostars synthesized at 5 °C were found to be significantly smaller (F-test,  $\alpha = 0.05$ ), than those of nanostars synthesized at 25 °C. The smaller standard deviation in plasmon position and spectral width at 5 °C compared to 25 °C support the argument that nanostars made at 5 °C had more reproducible plasmon bands than those made at 25 °C. Trials 1-3 used the same stock solutions of gold chloride, gold seed particles, ascorbic acid, and AgNO<sub>3</sub>. Trial 4 used a different batch of stock reagents and was conducted a week later to ensure and give more confidence to the reproducibility at 5 °C.

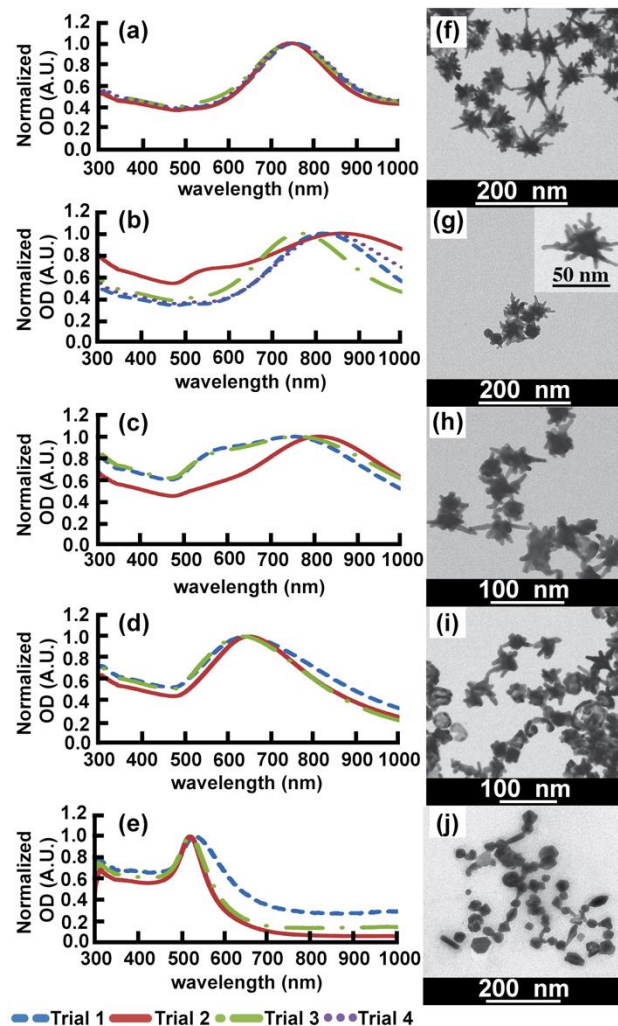


**Figure 1.** Normalized optical density (OD) showing the reproducibility of the plasmon resonance bands and TEM images showing the morphology of the gold nanostars when prepared at different temperatures: (a, f) 5 °C, (b, g) 25 °C, (c, h) 40 °C, (d, i) 50 °C, and (e, j) 90 °C. All experiments were conducted in triplicate except for 5 °C and 25 °C with  $n = 4$ . Notice 1a for 5 °C has better reproducibility in terms of plasmon peak position and spectral width at three quarters full maximum than the other temperatures.

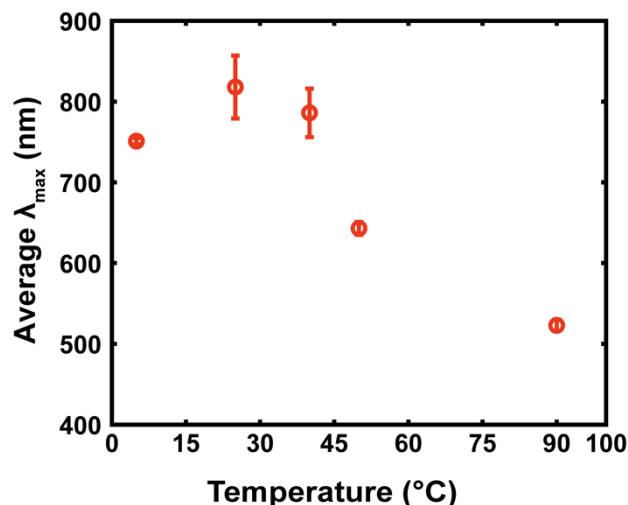


**Figure 2.** Average and Standard Deviation of the peak plasmon resonance wavelength ( $\lambda_{\max}$ ) from nanostars synthesized at different temperatures ( $n = 3$ , except for the nanostars at 5 and 25 °C with  $n = 4$ ). The 5 °C has the lowest error out of all the synthesis temperatures. Error bars represent  $\pm$  one standard deviation unit; some error bars are the same size or smaller than the symbol.

To further explore the nature of the plasmon reproducibility we examined the length of the spikes protruding from the gold nanosphere core. From the TEM images in Figure 1 and some that were not shown, the core diameter, spike length, tip-to-tip distance, and aspect ratio were measured as described in the experimental. The cores of the nanostars made at 5 and 25 °C were statistically similar in both the average and standard deviation:  $31.0 \pm 3.0$  nm ( $n = 10$ ) and  $33.0 \pm 5.0$  nm ( $n = 10$ ), respectively. The nanostars made at 5 °C had long spikes with an average length of about  $28.5 \pm 7.9$  nm ( $n = 20$ ) as seen in Figure 1(f). These spikes were statistically longer ( $\alpha = 0.05$ ) than the spikes on the 25 °C nanostars ( $21.8 \pm 9.2$  nm ( $n = 20$ )). The inset of Figure 1(g) shows that nanostars made at 25 °C also had side branches. The tip-to-tip distance of the nanostars is a critical feature for biomedical applications as they give vital information about the size of the particles and thus their usefulness in biological environments. When synthesized at 5 °C and 25 °C, the average tip-to-tip distances were  $81.9 \pm 8.2$  nm ( $n = 10$ ) and  $72.8 \pm 20.5$  nm ( $n = 10$ ), respectively. The standard deviation of the tip-to-tip distance was statistically smaller at 5 °C than 25 °C ( $\alpha = 0.05$ ). The aspect ratio ( $\frac{\text{Spike Length}}{\text{Spike Width}}$ ) of the spikes is integral to the plasmon band

position. The average aspect ratio for nanostars synthesized at 5 °C was  $2.58 \pm 0.89$  ( $n = 32$ ). Those synthesized at 25 °C had an average aspect ratio of  $3.35 \pm 1.12$  ( $n = 11$ ). The aspect ratio was statistically smaller ( $\alpha = 0.05$ ) in the nanostars made at 5 °C than those at 25 °C. The differences in aspect ratio likely play a key role in the plasmon peak position differences between the nanostars made at different temperatures. The lower standard deviation in the tip-to-tip distance of the nanostars synthesized at 5 °C was suspected to contribute to the reproducible  $\lambda_{\max}$  position, spectral shape, and spectral width.

Figures 1(c) and 2 show that the nanostars made at 40 °C had an average  $\lambda_{\max}$  of 786 nm and a large standard deviation of  $\pm 30$  nm ( $n = 3$ ). The average spectral width at 40 °C was about  $353 \pm 72$  nm ( $n = 3$ ) and varied from 272 nm to 410 nm. The large standard deviation of the  $\lambda_{\max}$  and spectral width show that the plasmons from nanostars synthesized at 40 °C were not reproducible. The approximately 20 % variability in the width of the spectral profile was a result of the heterogeneity of the shapes produced. Figure 1(h) reveals that some of the nanostars had just one or two spikes off the core. Of the spikes that could be measured, the average length was  $17.5 \pm 7.4$  nm ( $n = 20$ ) and was not statistically different from the spikes exhibited by the nanostars synthesized at 25 °C, but statistically smaller than those made at 5 °C ( $\alpha = 0.05$ ). The nanostar core diameters and tip-to-tip distances from the 40 °C synthesis were  $23.8 \pm 5.3$  nm ( $n = 10$ ) and  $53.9 \pm 15.4$  nm ( $n = 10$ ), respectively. The average core diameters and tip-to-tip distances were statistically smaller than those of both the 5 and 25 °C syntheses ( $\alpha = 0.05$ ). The standard deviation of the tip-to-tip distance for the nanostars made at 40 °C was statistically larger than that of the nanostars made at 5 °C ( $\alpha = 0.05$ ).

As the temperature increased past 40 °C the plasmon continued to blue shift (with respect to synthesis at 25 °C) and various shapes of nanoparticles were formed. Figures 1(d) and 2 show the nanoparticles made at 50 °C exhibit an average  $\lambda_{\max}$  of 643 nm corresponding to a blue shift of about 175 nm. Figure 1(i) shows the material produced from synthesis at 50 °C was a mixture of nanostars and other nanoparticle geometries. Figure 1(j) for synthesis at 90 °C shows that many more nanoparticle geometries were produced (nanorods, nanospheres, nanocubes etc.). Figure 3 shows

that the nanomaterial synthesized at 90 °C had a  $\lambda_{\text{max}}$  near 523 nm and was very similar to that of the gold seed particle solution.

From Figures 1(d), 1(e), and 2 for 50 and 90 °C, the standard deviations ( $n = 3$ ) were lower at  $\pm 8$  and  $\pm 7$  nm, respectively. While the  $\lambda_{\text{max}}$  position was reproducible for both 50 and 90 °C, the spectral shapes and widths were not very reproducible (Figure 1(d) and 1(e)). At 50 °C the spectral widths ranged from 186 nm to 238 nm and gave an average width of  $211 \pm 26$  nm ( $n = 3$ , 12 % RSD). The width for the 90 °C reaction ranged from 54 nm to 96 nm and averaged at  $71 \pm 22$  nm ( $n = 3$ ) with a 31 % RSD. The variation in peak shape and width was most likely due to the mixture of nanostars and other nanoparticle geometries present at these higher synthesis temperatures.

As the reaction temperature increased past 40 °C the pink gold chloride solution containing seed particles gradually became clearer. However, as the temperature increased past 70 °C, the solution gradually became pinker again. At both 50 and 90 °C, the reaction appeared to finish within a second. The 50 °C reaction occurred as expected, producing a solution with a dark blue-grey/green tint. In the 90 °C reaction, upon addition of the ascorbic acid and the  $\text{AgNO}_3$ , a dark pink/purple color was observed. The observed colors correlated well with the observed plasmon  $\lambda_{\text{max}}$  values of 643 nm and 523 nm at 50 °C and 90 °C, respectively. After centrifugation, the 50 °C had a slightly blue colored supernatant, but the 90 °C reaction had a slightly pink supernatant. The 90 °C reaction had a pellet that appeared both pink and dark blue.

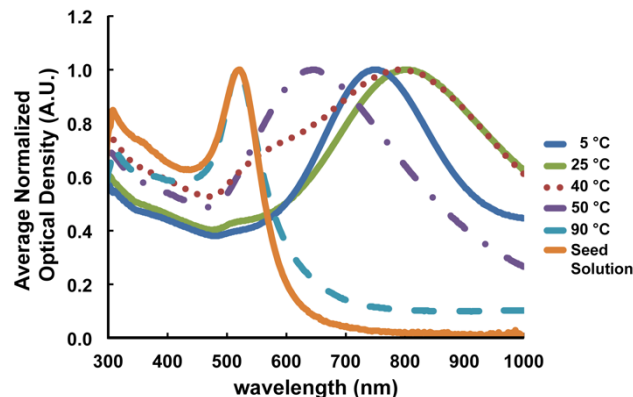


**Figure 3.** Average normalized optical density of plasmon bands from nanomaterial synthesized at each temperature as well as that of the seed solution (gold nanospheres). Notice the plasmon peak red shifts from the seed solution with addition of  $\text{AgNO}_3$  and ascorbic acid. The extent of the red shift depended on temperature with the 25 °C synthesis temperature showing the greatest red shift.

To summarize the data so far, synthesis at 5 °C gave nanostars with the best reproducibility in terms of standard deviation of the plasmon peak position ( $\lambda_{\text{max}}$ ), spectral width, and tip-to-tip distance (Figures 1, 2, and 3). While the 25 °C synthesis yielded nanostars, the  $\lambda_{\text{max}}$ , spectral width, and tip-to-tip distance were not reproducible. At temperatures between 40 °C and 90 °C, a mixture of gold nanostars and many kinds of nanoparticles were produced. The nanostars at 40 °C and 50 °C did not have very well defined spikes and often contained other nanoparticle geometries. No nanostars were observed at 90 °C. Instead, a variety of nanoparticle geometries were made. Figure 2 helps summarize the data according to reproducibility of the average and standard deviation of the plasmon  $\lambda_{\text{max}}$ . Figure 3 displays the nanostars  $\lambda_{\text{max}}$  position and spectral profile as a function of temperature and how the  $\lambda_{\text{max}}$  of the nanostars related to that of the seed solution. Formation of nanostars caused a red shift in the plasmon resonance with respect to the seed solution. As the synthesis temperature deviates from 25 °C, the nanostar  $\lambda_{\text{max}}$  blue shifts back toward that of the seed solution. The remainder of the discussion will focus on 5 and 25 °C syntheses because those temperatures yielded more nanostars than the other temperatures.

### ***Au (III) to Au (0) Conversion Yield***

The extinction peak at 306 nm from gold chloride was monitored before and after nanostar synthesis to determine the conversion yield of Au (III) to Au (0) (see experimental for more detail on the procedure). The conversion yield for synthesis at 5 °C and 25 °C were  $92.1 \pm 2.1 \%$  ( $n = 3$ ) and  $89.5 \pm 1.4 \%$  ( $n = 3$ ), respectively. These differences were not significantly different ( $\alpha = 0.05$ ).

### ***Tuning Plasmon Resonance with the AgNO<sub>3</sub> Concentration at 5 and 25 °C***

Nanostars exhibit  $\lambda_{\text{max}}$  values in the NIR region and are thus highly valuable in a variety of biological applications. Depending on the particular biological application or light source used, different  $\lambda_{\text{max}}$  values may be needed. Adjusting the AgNO<sub>3</sub> concentration has been shown to tune the  $\lambda_{\text{max}}$  to desired values.<sup>1</sup> The 5 °C synthesis was tested at different AgNO<sub>3</sub> concentrations to see if the plasmon band could still be tuned and maintain reproducibility when compared to the 25 °C synthesis.

All the data presented so far used a final concentration of 30  $\mu\text{M}$  AgNO<sub>3</sub> in the reaction vessel. We will now use the nomenclature S30 to refer to nanostars made using a final AgNO<sub>3</sub> concentration of 30  $\mu\text{M}$ , S20 to refer to a final AgNO<sub>3</sub> concentration of 20  $\mu\text{M}$ , and S35 to refer to a final AgNO<sub>3</sub> concentration of 35  $\mu\text{M}$ . As seen in Figure 4 and Figure S1, adjusting the AgNO<sub>3</sub> concentration under 5 °C synthesis conditions still allowed tuning of the plasmon band to a desired  $\lambda_{\text{max}}$  position. Use of 20  $\mu\text{M}$  AgNO<sub>3</sub> in the reaction yielded nanostars with a plasmon band at  $671 \pm 6$  nm ( $n = 3$ ) when synthesized at 5 °C. The plasmon  $\lambda_{\text{max}}$  had a statistically smaller standard deviation for the S20 nanostars made at 5 °C compared to the standard deviation of  $\pm 41$  nm ( $n = 3$ ) for S20 nanostars synthesized at room temperature (F-Test,  $\alpha = 0.05$ ).

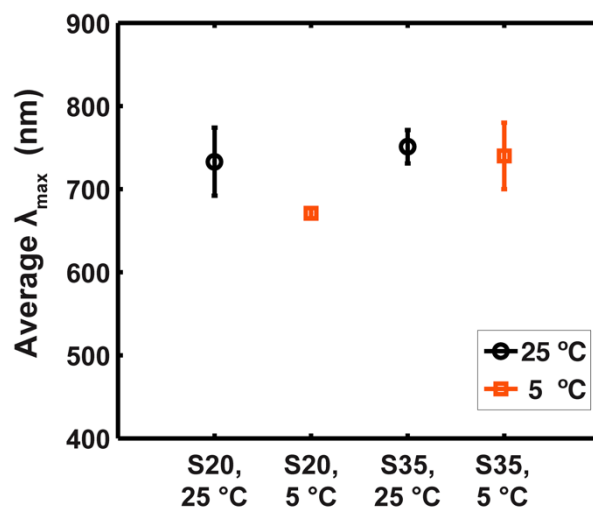


**Figure 4.** Average plasmon  $\lambda_{\max}$  of nanostars made at different  $\text{AgNO}_3$  concentrations and temperatures. S20 ( $n = 3$ ) nanostars used  $20 \mu\text{M}$   $\text{AgNO}_3$  for synthesis and S35 ( $n = 3$ ) used  $35 \mu\text{M}$   $\text{AgNO}_3$  for synthesis (all concentrations were the final concentration in reaction vessel). Synthesis of S20 nanostars at a reaction temperature of  $5^\circ\text{C}$  gave a statistically smaller ( $\alpha = 0.05$ ) standard deviation in the  $\lambda_{\max}$ , by a factor of 6.5, than S20s made at room temperature. The standard deviation of the  $\lambda_{\max}$  for S35s made at  $5^\circ\text{C}$  was not statistically different from that of the room temperature (F-test,  $\alpha = 0.05$ ). Therefore, both the S35s made at room temperature and at  $5^\circ\text{C}$  were not very reproducible. The error bar for the S20s at  $5^\circ\text{C}$  were the same size or smaller than the symbol, error bars represent  $\pm$  one standard deviation unit.

No further red shift in the  $\lambda_{\max}$  with respect to seed solution was observed after adding  $\text{AgNO}_3$  with a concentration greater than  $30 \mu\text{M}$  (Figures 4 and Figure S1). Instead the average  $\lambda_{\max}$  of nanostars with  $35 \mu\text{M}$   $\text{AgNO}_3$  appeared to blue shift with respect to S30s, but the average  $\lambda_{\max}$  was not reproducible and the extent of blue shift could not be precisely determined due to the large standard deviation (Figure 4 and Figure S1 of supporting information). We found no statistical difference ( $\alpha = 0.05$ ) from an F-test comparing the standard deviations of S35 nanostars at room temperature to those at  $5^\circ\text{C}$ . Therefore, neither the synthesis of S35s at room temperature nor at  $5^\circ\text{C}$  gave very reproducible plasmons.

Work by Fales *et al.* showed that gold nanostars coated with silver caused a significant blue shift with additional aliquots of  $\text{AgNO}_3$ .<sup>13</sup> If excess silver exists after the nanostar synthesis was complete, then it may have formed a silver coating. If a silver coating did form, then this would provide an explanation for the apparent blue

shift in the plasmon band of the S35 nanostars relative to the plasmon band of S30 nanostars. A blue shift from a silver coating would be expected as silver nanoparticles have  $\lambda_{\max}$  values near 425 nm.

Figures 5(a) and (b) show TEM images of the S20 nanostars at 25 °C and 5 °C, respectively. The tip-to-tip distance of the S20s at each temperature were about 60 nm and had about 35 nm cores. For both temperatures, the spikes of S30s were easier to see than those of the S20s (compare Figures 5(a) and (b) to Figures 1(f) and (g)).

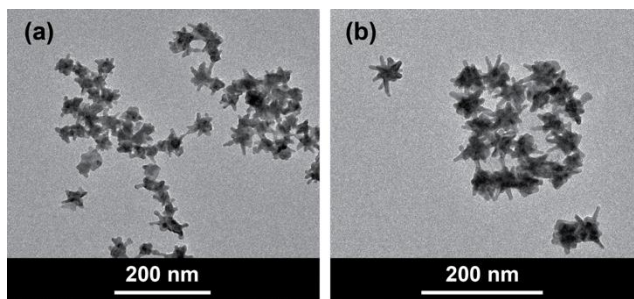


**Figure 5.** TEM image of S20 nanostars at (a) 25 °C and (b) 5 °C. The S20s at each temperature were about 60 nm tip-to-tip and had about 35 nm cores.

### ***Gold Nanostar Stability and Susceptibility to Aggregation***

The stability over time for the nanostars made at 5 °C was studied in DI water. Over the span of 21 days the  $\lambda_{\max}$  dropped from 737 nm to 699 nm (data not shown). After 21 days, the nanostars aggregated and crashed out of solution, rendering them useless. Because of this limited stability, nanostars are best used within a few weeks of synthesis when stored in DI water.

For the gold nanostars to function as an analytical tool, they need to be stable and resist aggregation in solution. The aggregation state of the nanostars is heavily influenced by the ionic strength of the solution. Even small changes to the local ionic environment of the nanostars will cause significant changes in the nanostar aggregation state.

The susceptibility of nanostars to aggregation was studied by changing the NaCl salt concentration in a method adapted from the work of Levy *et al.*<sup>35</sup> Two of the authors, Jacob Ramsey (JR) and Lixia Zhou (LZ), each synthesized nanostars at 5 °C

and 25 °C. After synthesis, all nanostar solutions were adjusted to  $1 \times 10^{10}$  nanostars/mL with increasing NaCl concentrations of 0, 15, 30, 75, and 150 mM.

Aggregation Potential was measured using the peak optical density (OD) ratio (Equation 1) and shift in the peak plasmon wavelength,  $\Delta\lambda_{\max}$  (Equation 2). The ‘x M NaCl’ in equations 1 and 2 corresponds to the different salt concentrations investigated (0 to 150 mM NaCl). An aggregation potential of zero for either metric indicated no aggregation. Deviations from zero represent a change in the aggregation state of the nanostars. Figure 6 (a) and (b) show that the nanostars aggregated as the salt concentration was increased. For nanostars made at 5 and 25 °C, the aggregation potential steadily increased from the 0 to 30 mM NaCl. At 75 mM and beyond the aggregation potential plateaued. From range finding experiments to determine NaCl concentrations to use (data not shown), we found all solutions visibly changed color from a dark green/blue hue to a more clear blue hue at 50 mM NaCl.

$$\text{OD ratio} = \frac{\text{OD}_{\max}(0 \text{ M NaCl}) - \text{OD}_{\max}(x \text{ M NaCl})}{\text{OD}_{\max}(0 \text{ M NaCl})} \quad (1)$$

$$\Delta\lambda_{\max} = \lambda_{\max}(0 \text{ M NaCl}) - \lambda_{\max}(x \text{ M NaCl}) \quad (2)$$

The aggregation potential of the nanostars made at 5 and 25 °C behaved differently when looking at both the peak optical density ratio and plasmon  $\lambda_{\max}$  shift. For nanostars prepared by each author (JR and LZ), as the salt concentration increased, the aggregation potential increased faster for the nanostars made at 25 °C than the 5 °C. This effect was much more noticeable when looking at the  $\Delta\lambda_{\max}$  rather than the OD ratio. Since each author (JR and LZ) independently made the same observation regarding the aggregation potential, we concluded that nanostars made at 5 °C were less susceptible to aggregation than the nanostars made at 25 °C for salt concentrations less than 75 mM.

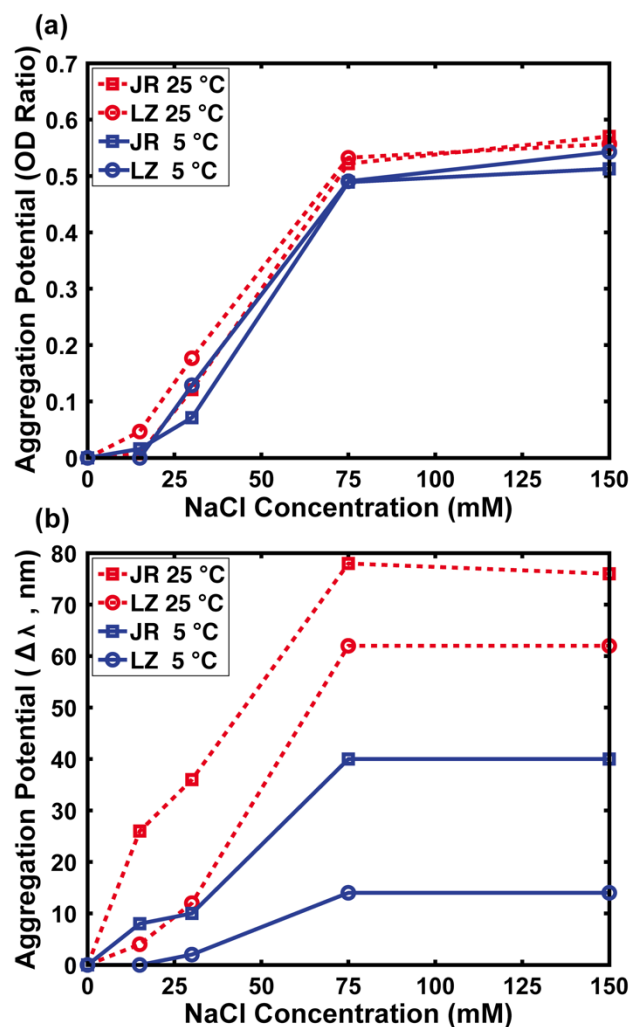


**Figure 6.** Aggregation potential of nanostars made at 5 and 25 °C. Trials were performed by two of the authors (Jacob Ramsey (JR) and Lixia Zhou (LZ)) and similar trends were observed from nanostars prepared by both authors. The gold nanostar aggregation potential as (a) the peak optical density ratio and (b) the shift in plasmon  $\lambda_{\max}$ , ( $\Delta\lambda_{\max}$ ) vs. NaCl concentration (0, 15, 30, 75, and 150 mM). Below 75 mM NaCl, nanostars made at 5 °C demonstrated less potential for aggregation than those made at 25 °C (compare nanostars made by each author at the two temperatures).

### *Investigation of Reaction Time at 5 °C*

According to one study done by Yuan *et al.*, the reaction at room temperature was complete within 30 seconds after the addition of Ascorbic Acid and  $\text{AgNO}_3$ .<sup>1</sup> We observed that as the reaction occurred at 25 °C, the color changed from light pink to a dark blue-gray over 3 - 5 seconds. At 5 °C, the solution started out a light pink and then slowly turned to a light gray, then to a dark gray, and then to a deep blue-gray.

This color change took 10 - 30 seconds, indicating that the reaction may take longer to complete at lower temperatures. We suspected the lower temperature might slow down reduction of gold onto the nanosphere surface allowing for a more controlled, reproducible growth of the spikes. At 5 °C we hypothesized that if the reaction does not complete in 30 seconds, then the  $\lambda_{\text{max}}$  should shift relative to the 30 second time point as more gold gets deposited onto the nanospheres with longer reaction times.

To test this hypothesis a time study at 5 °C was performed. We let the reaction occur for 30, 60, 120, and 300 seconds. Allowing the reaction to occur for longer than 30 seconds did not show any statistically significant change in  $\lambda_{\text{max}}$  from the 30-second time point (Figure S2 of supporting information). From these results, we have shown that the reaction time, past 30 seconds, did not influence the  $\lambda_{\text{max}}$  of the nanostars.

The standard deviation of all the time trials at 5 °C was about  $\pm 14$  nm ( $n = 12$ ). This was still statistically smaller (F-Test,  $\alpha = 0.05$ ) than the  $\pm 39$  nm ( $n = 4$ ) standard deviation of the reaction at 25 °C. Thus, not only did the temperature-mediated method yield reproducible nanostars, but the nanostars were also reproducible across different reaction times. The average  $\lambda_{\text{max}}$  for all reaction times was 708 nm, about 40 nm lower than expected. The reason for this had to do with the stability of the gold chloride reagent and not the reaction temperature. These shifts in plasmon  $\lambda_{\text{max}}$  due to the reagent will be elaborated on in the following sections.

### ***Concentration Matching Gold Nanostar Samples***

While the  $\lambda_{\text{max}}$  was found to be reproducible in gold nanostars synthesized at 5 °C, the raw intensity of the optical density was not always consistent. Using a Nanosight instrument, we were able to obtain an approximate concentration of the nanostars to prepare concentration matched solutions for analysis of the optical density and extinction coefficients of the nanostars plasmon bands. The reader should note that the Nanosight concentration estimates are approximate values, and these values are not the most accurate. Atomic emission or other similar methods will give a more accurate estimate of the concentrations. However, provided the instrument acquisition settings remain unchanged for analysis of different samples, the Nanosight is precise enough to

compare the relative concentrations of each synthesis trial used in the concentration matching experiments.

Nanostars were synthesized at 5 and 25 °C in triplicate at each temperature. Figure S3 in the supporting information shows the concentration matched plasmon bands of gold nanostars for both 25 °C (Figure S3a) and 5 °C (Figure S3b). Prior to dilution of the nanostars synthesized at 5 °C, the peak optical density values were 2.554, 2.798, and 2.728. This gave an average of 2.693 with a standard deviation of  $\pm 0.126$ . Using the Nanosight data, we were able to approximately match the concentrations to  $1.25 \times 10^{11}$  nanostars/mL. The optical densities of concentration matched nanostars were 2.358, 2.540, and 2.395. The average optical density was  $2.431 \pm 0.096$ .

For the synthesis at 25 °C, the optical densities were 2.882, 1.768, and 2.046. This gave an average optical density of 2.232 with a standard deviation of  $\pm 0.580$  prior to concentration matching. After matching the concentrations to  $4.74 \times 10^{10}$  nanostars/mL, the optical densities were 2.031, 1.629, and 1.894 giving an average optical density  $1.851 \pm 0.204$ . Although the optical densities can vary after initial synthesis at both temperatures, we have demonstrated the ability to control the concentration of these nanoparticles in solution after their initial synthesis.

Extinction coefficients are wavelength dependent but not concentration dependent. Since the Nanosight and UV/Vis acquisition settings were the same for nanostars made at both temperatures, a statistical comparison of the extinction coefficients was possible. Six solutions were analyzed at each temperature (three unmatched and three matched concentrations). Comparison of the extinction coefficients between the different nanostar solutions must be done at the same  $\lambda_{\max}$ . For each temperature investigated, the extinction coefficient was determined for each solution, resulting in six extinction coefficients at each of the six  $\lambda_{\max}$  values. There was no statistical difference ( $\alpha = 0.05$ ,  $n = 6$ ) between the extinction coefficients of the unmatched and matched concentration solutions at each of the six  $\lambda_{\max}$  values for either of the temperatures investigated. This result was expected as the extinction coefficient is independent of the concentration. Furthermore, the extinction coefficients could be used, cautiously, to estimate nanostar concentration based on optical density at a given wavelength.

At each  $\lambda_{\max}$  value the extinction coefficients of the matched and unmatched concentrations were pooled to find the average extinction coefficients for the 5 and 25 °C nanostars. The average extinction coefficients for the 5 °C nanostars ranged from  $1.932 \pm 0.194 \times 10^{-11} \frac{\text{cm}^2}{\text{particle}}$  (10. % RSD) at 748 nm to  $1.995 \pm 0.113 \times 10^{-11} \frac{\text{cm}^2}{\text{particle}}$  (5.7 % RSD) at 718 nm (n = 6). The average extinction coefficients for the 25 °C nanostars ranged from  $3.765 \pm 0.306 \times 10^{-11} \frac{\text{cm}^2}{\text{particle}}$  (8.1 % RSD) at 930 nm to  $3.811 \pm 0.353 \times 10^{-11} \frac{\text{cm}^2}{\text{particle}}$  (9.3 % RSD) at 898 nm (n = 6).

To compare the average extinction coefficients, the 720 nm plasmon wavelength was chosen because it fell within the plasmon bands of both the 5 and 25 °C nanostars. The average extinction coefficients for the 5 and 25 °C nanostars were  $1.995 \pm 0.119 \times 10^{-11} \frac{\text{cm}^2}{\text{particle}}$  (5.9 % RSD) and  $2.341 \pm 0.276 \times 10^{-11} \frac{\text{cm}^2}{\text{particle}}$  (12 % RSD), respectively (n = 6). The average extinction coefficients at 5 and 25 °C were statistically different ( $\alpha = 0.05$ ). The difference in the average extinction coefficients at 720 nm for the 5 and 25 °C nanostars indicates that there were fundamental differences in the geometric and plasmonic properties of the nanostars made at the two temperatures. Similar comparisons and results were made for the average extinction coefficient at each  $\lambda_{\max}$  value, but the confidence level varied from  $\alpha = 0.001$  to  $\alpha = 0.10$  (data not shown).

Since the extinction coefficient is wavelength dependent the average extinction coefficients from each  $\lambda_{\max}$  could not be averaged together to get a standard deviation. Instead the standard deviation of the extinction coefficient at each  $\lambda_{\max}$  value was averaged to compare average standard deviations between 5 and 25 °C. The average standard deviation of the extinction coefficient was shown to be statistically smaller ( $\alpha = 0.05$ , n = 6) for the nanostars synthesized at 5 °C compared to nanostars synthesized at 25 °C. This provides additional support that nanostars synthesized at 5 °C were more reproducible. Both the 5 and 25 °C synthesis showed average  $\lambda_{\max}$  values about 40 and 70 nm, respectively, away from those previously discussed. The reason for this shift in wavelength will be discussed in detail below.

### ***Proper Reagent Care and the Influence on Synthesis***

While synthesizing biocompatible gold nanostars at 5 °C, we found it essential to take great care of the gold chloride. It must be kept in a very dry environment and protected from air to prevent the gold from being reduced or further hydrated. We found that if the gold chloride was in use for several months, or left out of the desiccator, then the nanostar plasmon bands were blue shifted relative to nanostars synthesized with a previously unopened bottle of gold chloride. While the plasmon band exhibited a shift, the gold nanostars made at 5 °C were still reproducible at the new  $\lambda_{\max}$  (Figure S2). We suspect this shift to be a result of trace reducing agents in the air reacting with water and gold to alter the oxidation state of the gold prior to use for synthesis. The gold chloride, when left outside a desiccator, or even left in solution, will influence the nanostar synthesis. We recommend using the gold chloride solution immediately after its preparation. If proper care is kept of the gold chloride reagent, then gold nanostars with a reproducible  $\lambda_{\max}$  will continue to be produced. For care of the solid gold chloride, we recommend sealing the lid with parafilm wax to protect from reducing agents in the air, wrapping tin foil around the bottle to protect from light, and placing the bottle in a desiccator to protect from water.

### ***Validation of Nanostar Plasmon Reproducibility from Synthesis at 5 °C***

Throughout this work, the plasmon  $\lambda_{\max}$  values shifted for syntheses at both 5 and 25 °C. For each temperature, plasmon UV/Vis data from the nanostars made by each author, JR and LZ, were pooled to validate that the 5 °C synthesis actually produced more reproducible plasmon bands than those made at 25 °C. In doing so we found the average plasmon  $\lambda_{\max}$  was  $718.4 \pm 26.6$  nm ( $n = 27$ ) and  $818.9 \pm 68.5$  nm ( $n = 15$ ) for the 5 and 25 °C, respectively. From an F-test ( $\alpha = 0.05$ ) the standard deviation from synthesis at 5 °C was statistically smaller and thus more reproducible.

Figure 7 shows a box and whisker plot of the pooled nanostar data for synthesis at 5 and 25 °C. These plots show the broad range of values for  $\lambda_{\max}$  for nanostars made at 25 °C compared to 5 °C. The  $\lambda_{\max}$  values for nanostars synthesized at 25 °C span almost 150 nm compared to about 50 nm for nanostars synthesized at

5 °C. The tighter distribution of data in the 5 °C nanostars showed a higher degree of reproducibility than was achieved with the broad ranging 25 °C nanostars.

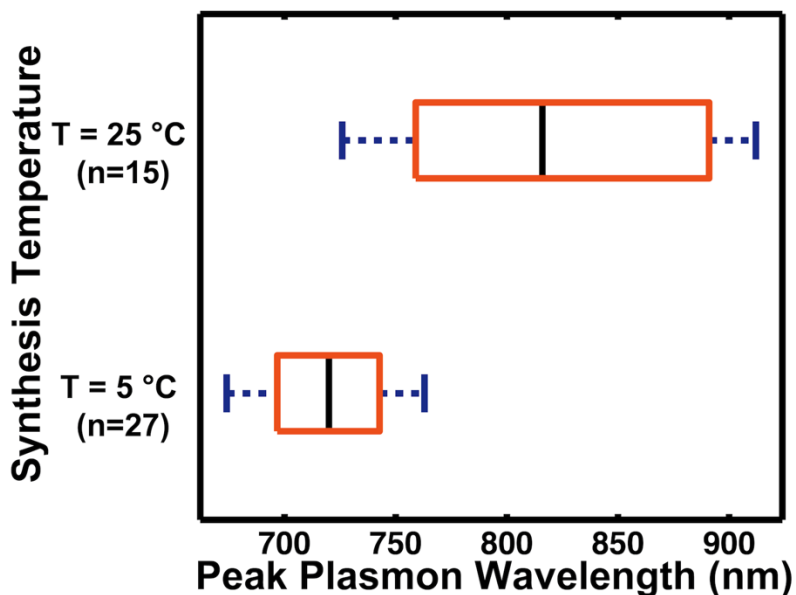


**Figure 7.** Box and Whisker plot of pooled nanostar plasmon data from authors JR and LZ to compare plasmon  $\lambda_{\max}$  reproducibility of the synthesis at 5 °C, n = 27 and 25 °C, n = 15. Pooling the data from each author helped validate that the 5 °C nanostar synthesis gave more reproducible peak plasmon wavelengths than the synthesis at 25 °C.

## CONCLUSION

In conclusion, a method for 5 °C temperature/seed-mediated synthesis of biocompatible gold nanostars with reproducible plasmon bands and spectral widths has been presented. The novelty of the temperature-mediated synthesis lies in the reproducibility of the spectral response. Another novelty of the approach is the use of temperature to tune the plasmon band in addition to changing the  $\text{AgNO}_3$  concentration. The low temperature nanostar synthesis kept the plasmons in the NIR region making the nanostars ideal for bioanalytical and other biological applications.

A lower standard deviation in the  $\lambda_{\max}$  corresponded to greater reproducibility of the spectral response from the nanostars. While synthesis at 25 °C produced nanostars with  $\lambda_{\max}$  values in the NIR region, it could not do so in a reproducible manner. The standard deviation of the plasmon  $\lambda_{\max}$  values from synthesis at 5 °C under two different  $\text{AgNO}_3$  concentrations was found to be statistically smaller than those of the synthesis at 25 °C. While the plasmon band varied depending on the age

of the gold chloride and the person making the nanostars at both 5 and 25 °C, on average the 5 °C synthesis proved more reproducible.

We suspect the reproducible plasmon peaks were the result of altered reaction conditions at 5 °C that provided more control over the synthesis to produce, on average, a more homogenous distribution of nanostars with more reproducible spike characteristics. Future studies are planned to elucidate the nature of the reproducibility and study the synthetic mechanism to understand how the synthesis changed at 5 °C. We also plan to use the reproducible/tunable gold nanostars in the future for sensitive and reproducible Surface Enhanced (Resonant) Raman Scattering biosensors.

## SUPPLEMENTAL INFORMATION

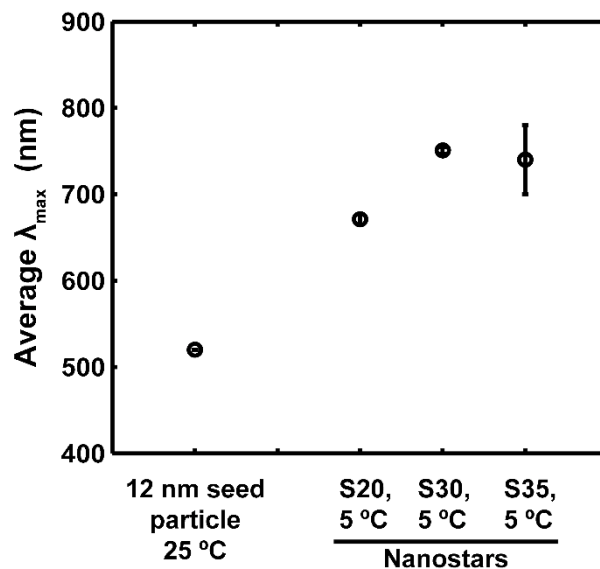


**Figure S1.** Average plasmon  $\lambda_{\max}$  as a function of silver concentration during nanostar synthesis at 5 °C and comparison to the seed solution. S20 (n = 3) nanostars used 20  $\mu\text{M}$   $\text{AgNO}_3$  for synthesis, S30 (n = 4), used 30  $\mu\text{M}$   $\text{AgNO}_3$  for synthesis, and S35 (n = 3) used 35  $\mu\text{M}$   $\text{AgNO}_3$  for synthesis (all concentrations were the final concentration in reaction vessel). The average  $\lambda_{\max}$  red shifts with respect to the seed solution (n = 4) as silver content was increased during synthesis. Beyond 30  $\mu\text{M}$   $\text{AgNO}_3$  no significant red shift was observed and reproducibility of  $\lambda_{\max}$  was lost at 5 °C. Error bars represent  $\pm$  one standard deviation unit; in some cases the error bars are the same size or smaller than the symbol.

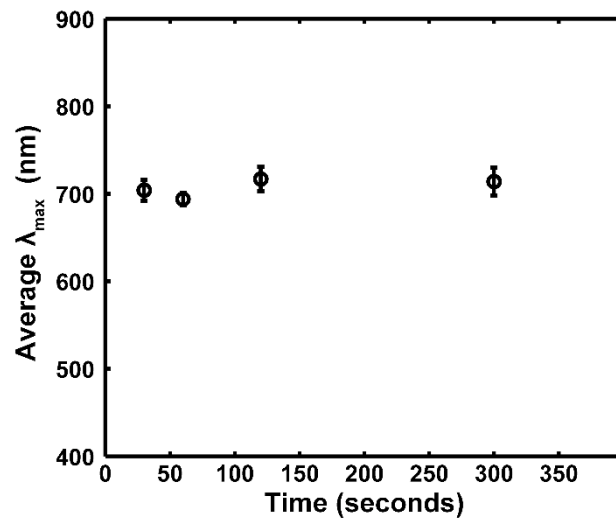


**Figure S2.** Plot of the S30 nanostars average  $\lambda_{\text{max}}$  vs. reaction time in seconds. No statistical difference in the average  $\lambda_{\text{max}}$  was observed between the time points. We concluded from this data that the reaction was complete within the first 30 seconds. The error bars represent  $\pm$  one standard deviation unit ( $n = 3$ ); in some cases the error bars were the same size as the symbol.

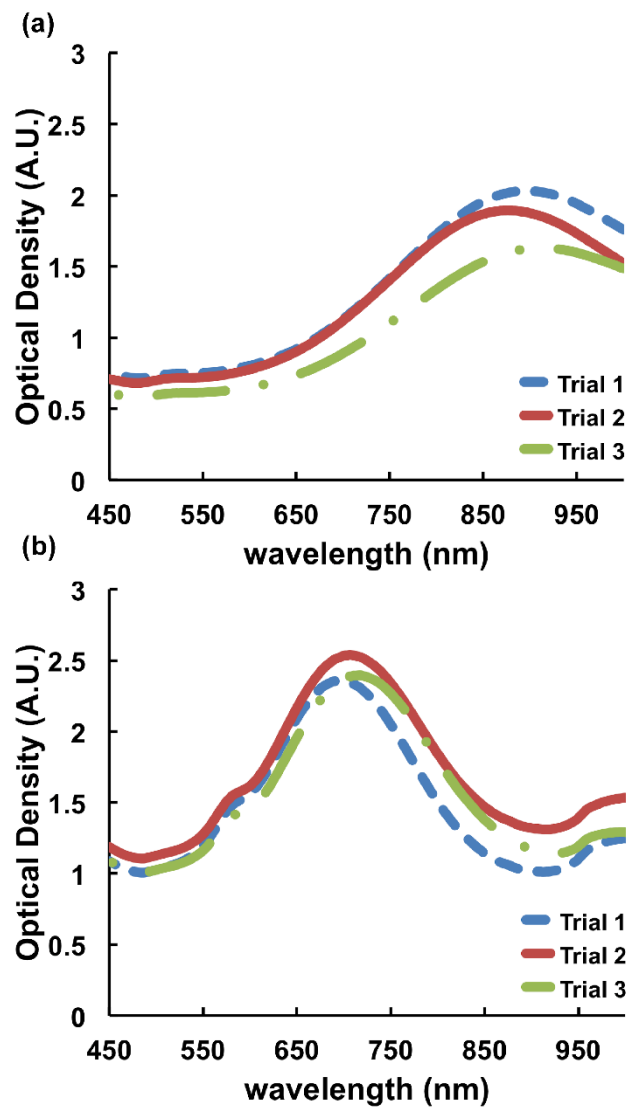


**Figure S3.** Concentration matched samples using data from Nanosight. (a) 25 °C nanostars showed similar optical density signals after diluting samples to the same concentration ( $4.74 \times 10^{10}$  nanostars/mL). (b) 5 °C nanostars showed similar optical density signals after diluting samples to the same concentration ( $1.25 \times 10^{11}$  nanostars/mL).

## REFERENCES

- 1 H. Yuan, C. G. Khoury, H. Hwang, C. M. Wilson, G. A. Grant and T. Vo-Dinh, *Nanotechnology*, 2012, **23**, 075102.
- 2 R. Alvarez-Puebla, L. M. Liz-Marzán and F. J. García de Abajo, *J. Phys. Chem. Lett.*, 2010, **1**, 2428–2434.
- 3 O. Bibikova, A. Popov, I. Skovorodkin, A. Prilepskyi, T. Pylaev, A. Bykov, S. Staroverov, V. Bogatyrev, V. Tuchin, M. Kinnunen, S. Vainio, K. Kordas and N. Khlebtsov, 2013, vol. 8801, pp. 880102–880102–8.
- 4 S. K. Dondapati, T. K. Sau, C. Hrelescu, T. A. Klar, F. D. Stefani and J. Feldmann, *ACS Nano*, 2010, **4**, 6318–6322.
- 5 L. Rodríguez-Lorenzo, R. A. Álvarez-Puebla, F. J. G. de Abajo and L. M. Liz-Marzán, *J. Phys. Chem. C*, 2010, **114**, 7336–7340.
- 6 S. Barbosa, A. Agrawal, L. Rodríguez-Lorenzo, I. Pastoriza-Santos, R. A. Alvarez-Puebla, A. Kornowski, H. Weller and L. M. Liz-Marzán, *Langmuir*, 2010, **26**, 14943–14950.
- 7 L. Shao, A. S. Susha, L. S. Cheung, T. K. Sau, A. L. Rogach and J. Wang, *Langmuir*, 2012, **28**, 8979–8984.
- 8 C. Hrelescu, T. K. Sau, A. L. Rogach, F. Jäckel, G. Laurent, L. Douillard and F. Charra, *Nano Lett.*, 2011, **11**, 402–407.
- 9 F. Hao, C. L. Nehl, J. H. Hafner and P. Nordlander, *Nano Lett.*, 2007, **7**, 729–732.
- 10 E. S. Allgeyer, A. Pongan, M. Browne and M. D. Mason, *Nano Lett.*, 2009, **9**, 3816–3819.
- 11 C. G. Khoury and T. Vo-Dinh, *J. Phys. Chem. C*, 2008, **112**, 18849–18859.
- 12 A. S. Thakor, J. Jokerst, C. Zavaleta, T. F. Massoud and S. S. Gambhir, *Nano Lett.*, 2011, **11**, 4029–4036.
- 13 A. M. Fales, H. Yuan and T. Vo-Dinh, *J. Phys. Chem. C*, 2014, **118**, 3708–3715.
- 14 H. Yuan, A. M. Fales, C. G. Khoury, J. Liu and T. Vo-Dinh, *J. Raman Spectrosc.*, 2013, **44**, 234–239.
- 15 S. C. Glotzer and M. J. Solomon, *Nat. Mater.*, 2007, **6**, 557–562.
- 16 H.-L. Wu, H.-R. Tsai, Y.-T. Hung, K.-U. Lao, C.-W. Liao, P.-J. Chung, J.-S. Huang, I.-C. Chen and M. H. Huang, *Inorg. Chem.*, 2011, **50**, 8106–8111.

- 17 M. Li, J. Zhang, S. Suri, L. J. Sooter, D. Ma and N. Wu, *Anal. Chem.*, 2012, **84**, 2837–2842.
- 18 B. L. Sanchez-Gaytan, Z. Qian, S. P. Hastings, M. L. Reca, Z. Fakhraai and S.-J. Park, *J. Phys. Chem. C*, 2013, **117**, 8916–8923.
- 19 D.-K. Lim, K.-S. Jeon, J.-H. Hwang, H. Kim, S. Kwon, Y. D. Suh and J.-M. Nam, *Nat. Nanotechnol.*, 2011, **6**, 452–460.
- 20 S. P. Hastings, P. Swanglap, Z. Qian, Y. Fang, S.-J. Park, S. Link, N. Engheta and Z. Fakhraai, *ACS Nano*, 2014, **8**, 9025–9034.
- 21 J. Xie, J. Y. Lee and D. I. C. Wang, *Chem. Mater.*, 2007, **19**, 2823–2830.
- 22 X.-L. Liu, J.-H. Wang, S. Liang, D.-J. Yang, F. Nan, S.-J. Ding, L. Zhou, Z.-H. Hao and Q.-Q. Wang, *J. Phys. Chem. C*, 2014, **118**, 9659–9664.
- 23 P. S. Kumar, I. Pastoriza-Santos, B. Rodríguez-González, F. J. G. de Abajo and L. M. Liz-Marzán, *Nanotechnology*, 2008, **19**, 015606.
- 24 A. Topete, M. Alatorre-Meda, E. M. Villar-Álvarez, A. Cambón, S. Barbosa, P. Taboada and V. Mosquera, *ACS Appl. Mater. Interfaces*, 2014, **6**, 11142–11157.
- 25 R. Sardar, A. M. Funston, P. Mulvaney and R. W. Murray, *Langmuir ACS J. Surf. Colloids*, 2009, **25**, 13840–13851.
- 26 A. J. Mieszawska, W. J. M. Mulder, Z. A. Fayad and D. P. Cormode, *Mol. Pharm.*, 2013, **10**, 831–847.
- 27 A. Casu, E. Cabrini, A. Donà, A. Falqui, Y. Diaz-Fernandez, C. Milanese, A. Taglietti and P. Pallavicini, *Chem. – Eur. J.*, 2012, **18**, 9381–9390.
- 28 P. Pallavicini, G. Chirico, M. Collini, G. Dacarro, A. Donà, L. D’Alfonso, A. Falqui, Y. Diaz-Fernandez, S. Freddi, B. Garofalo, A. Genovese, L. Sironi and A. Taglietti, *Chem. Commun.*, 2011, **47**, 1315–1317.
- 29 P. Pallavicini, A. Donà, A. Casu, G. Chirico, M. Collini, G. Dacarro, A. Falqui, C. Milanese, L. Sironi and A. Taglietti, *Chem. Commun.*, 2013, **49**, 6265–6267.
- 30 G. Cavallaro, D. Triolo, M. Licciardi, G. Giammona, G. Chirico, L. Sironi, G. Dacarro, A. Donà, C. Milanese and P. Pallavicini, *Biomacromolecules*, 2013, **14**, 4260–4270.
- 31 P. Dey, I. Blakey, K. J. Thurecht and P. M. Fredericks, *Langmuir*, 2013, **29**, 525–533.

- 32 J. R. G. Navarro, A. Liotta, A.-C. Faure, F. Lerouge, F. Chaput, G. Micouin, P. L. Baldeck and S. Parola, *Langmuir*, 2013, **29**, 10915–10921.
- 33 H. Yuan, Y. Liu, A. M. Fales, Y. L. Li, J. Liu and T. Vo-Dinh, *Anal. Chem.*, 2013, **85**, 208–212.
- 34 W. Callister, *Materials Science and Engineering An Introduction, (Pages 312-320)*, John Wiley & Sons, Inc., Seventh., 2007.
- 35 R. Lévy, N. T. K. Thanh, R. C. Doty, I. Hussain, R. J. Nichols, D. J. Schiffrin, M. Brust and D. G. Fernig, *J. Am. Chem. Soc.*, 2004, **126**, 10076–10084.

## Chapter 2

### Experiments in Metal Enhanced Fluorescence: Proof of Enhancement

(Some of the Data in this chapter are from the studies of Lixia Zhou)

## INTRODUCTION

The previous chapter discussed gold nanostars and why they are of interest in various fields. Our lab has researched in-depth many of the factors influencing gold nanostar synthesis, as seen in Chapter 1. The result has been a more robust synthesis technique leading to reproducible plasmon bands along with a greater understanding of the gold nanostar colloidal stability.<sup>1</sup> The field is currently limited by the lack of reproducible synthesis methods.<sup>2</sup> We first became interested in these particles due to their ability to be used as Surface Enhanced Raman Scattering (SERS) substrates and their high signal enhancement. Electrons in the conduction band of the gold nanostars form surface plasmons that resonate at a certain frequency depending on the size and shape of the particle and form surface plasmons.<sup>3</sup> These local surface plasmons give the nanostars a unique interaction with light. Our lab wants to utilize these plasmons to enhance Raman and fluorescence signals and increase the sensitivity of our biosensors.

The plasmonic properties of gold nanostars enhance the interaction of light with molecules near the nanostar's surface plasmons resulting in a signal enhancement effect that is distant dependent. This can be utilized in two different techniques: Metal Enhanced Fluorescence (MEF) and Surface Enhanced Raman Scattering.<sup>3,4</sup> This chapter will discuss gold nanostars and their use in Metal Enhanced Fluorescence. The synthesis technique developed in the previous chapter is an essential part of this study. The ability to obtain a reproducible analytical signal depends on the reproducibility of the nanoparticle plasmon as the plasmon is directly involved in enhancing the signal. In metal enhanced fluorescence, it is thought that the surface plasmons, when in close proximity (just over 20 nm) with a fluorescent dye, will increase the rates of excitation and emission thus increase the incidence of fluorescent emission.<sup>4</sup>

The overarching goal of the Burrows lab group is to develop innovative new DNA based biosensors to visualize microRNA's in cells and tissues (the importance of these microRNA's will be discussed in a later chapter). Fluorescence is a common technique currently used to interrogate these systems. In our studies, fluorescent dyes were electrostatically attached to the gold nanostar using an avidin/biotin system in

addition to DNA. Below, in Figure 2-1, is a schematic for the nanoassembly used in these studies.

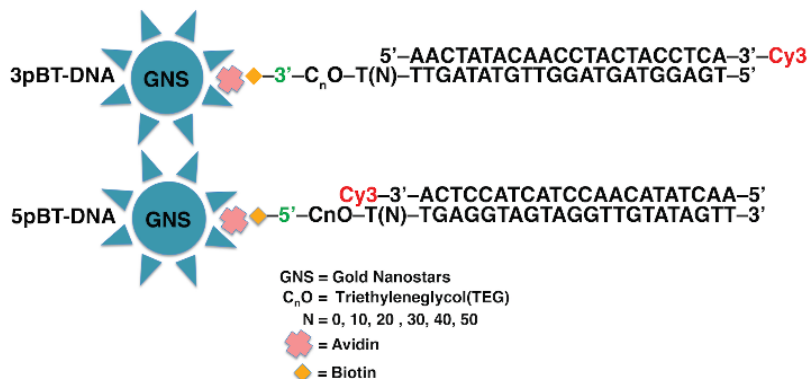


**Figure 2-1.** The schematic of the nanoassembly used in the MEF studies. Studies were performed with Cy3 on either the 5' or 3' end. Gold nanostars are coated with SDS and avidin and then bound to biotinylated DNA capture probe that is complimentary to a Cy3 reporter strand. Varying lengths of Thymine base pairs were used, T(N)" to adjust the dye distance from the nanostar.<sup>5</sup>

The enhancement of the fluorescence signal due to the close proximity of the dye to the nanostar is evident in Figure 2-2. Fluorescence was measured both on the gold nanostars and on similarly sized silica nanoparticles. The dye on the gold nanostars shows a clear signal enhancement over the dye on silica nanoparticles. Mechanistically, it was proposed by Lackowitz that an increased quantum yield of the system results from rapid energy transfer from the fluorophore to the plasmons, which then radiate to the far field.<sup>6</sup> Changes in transition lifetimes are known to play a role in the alteration of the quantum yield. Different metals, shapes, and thicknesses all affect whether fluorescence is quenched or enhanced.<sup>6</sup>

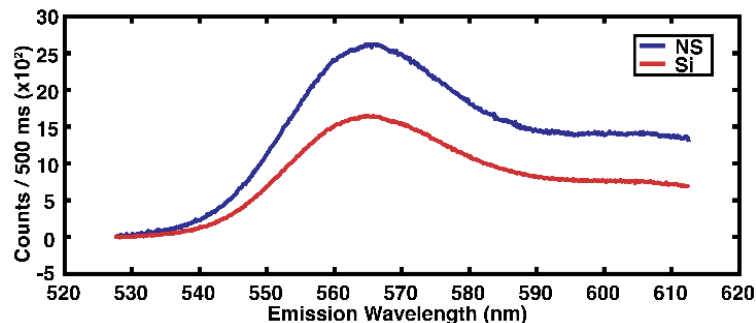


**Figure 2-2.** Enhanced Fluorescence from Cy3 on ~ 80 nm Gold Nanostars compared to fluorescence on 80nm Silica nanoparticles. GNS and silica nanoparticles were coated with avidin and 3pBT30Cy3 Pair. Cy3 was excited at 742 nm.<sup>5</sup>

In this study, free biotin was added to the nano-assembly to validate the biotinylated DNA was actually bound to the nanostar and showing MEF. Another reason for these experiments was to confirm that the enhanced fluorescence was not just due to the concentration of the dyes on the nanoparticle.

The pure biotin addition experiment takes advantage of small differences in avidin's affinity for pure biotin over modified biotin. Pure biotin will have a greater affinity for avidin than a biotinylated DNA molecule. The pure biotin complex with no modifications is expected to out-compete the biotinylated DNA for positions on the avidin. As a control, buffer with no biotin was added to the nano-assembly. The fluorescence of Cy3 before and after addition of biotin was monitored over time. If MEF was actually observed, then we expect to see a larger decrease in the fluorescence signal for the pure biotin addition compared to the control.

## EXPERIMENTAL

Gold nanostars were prepared via the synthesis technique described in Chapter 1. Gold nanostars were coated with Sodium Dodecyl Sulfate (SDS) and avidin. A 76 nM 5pBT0Cy3 (5' Biotin with 0 T spacer and 3' Cy3 Dye) solution was added to the nanostars. At the beginning of the study an initial fluorescence measurement was acquired. The decrease in fluorescence signal with addition of pure biotin was monitored over time. A Mai-Tai Tunable Laser was used for two-photon excitation at 742 nm. The laser power was set at 75 mW with 100 fs pulses at an 80 MHz repetition rate. Acquisition settings were 6 sets of 10 frames with 500 ms exposures, all averaged.

Free Biotin was added at 120 times excess (45.6 $\mu$ M) to the biotin-DNA-Cy3 complex. The fluorescence signal was taken initially at 0 minutes (before the addition of free biotin) and 1 minute post addition. Measurements were then taken every 2 minutes until 27 minutes post addition. The signal intensity was collected and monitored at 569.166 nm. As a control, we diluted a sample with just buffer so there was no addition of free biotin.

## **RESULTS AND DISCUSSION**

The addition of biotin was expected to displace the biotinylated, dye labeled DNA on the gold nanostars and cause a decrease in the signal. The signal was expected to decrease, because the dye was no longer in the proper proximity to the nanostar. The data shows that free biotin likely displaced the biotinylated DNA on the gold nanostar surface.

Figure 2-3 shows the decrease in fluorescence signal as time progressed post addition of free biotin to the sample. Upon addition of the free biotin to the nanostar solution, there was an immediate decrease in the signal at the first time point due to the dilution of the dye labeled nanoassembly by addition of the free biotin. The fluorescence signal continued to decrease for the next 10-30 minutes. The addition of just buffer (no free biotin), the control, also shows a decrease in fluorescence signal initially, but this was simply due to the dilution of the dye labeled nanoassembly. There was no further reduction in the signal post-dilution.

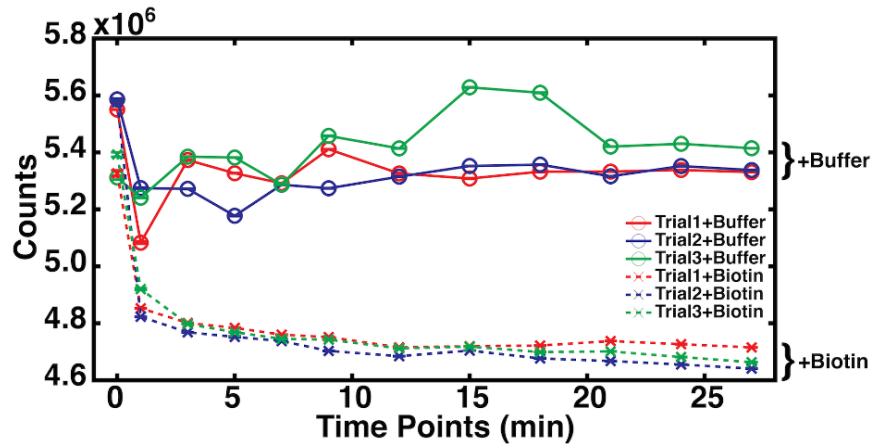


**Figure 2-3.** Cy3 Fluorescence evolution over time after dilution with buffer or addition of free biotin. The lower fluorescence of the biotin addition compared to the buffer demonstrates that the 5pBT0Cy3 DNA was displaced from the nanostar and provides evidence of MEF.<sup>5</sup>

The initial decrease in fluorescence signal was much greater in the trials where free biotin was added. Not only was the dye diluted, but Figure 2-3 provided strong evidence that the further decrease in fluorescence was due to the displacement of the 5pBT0Cy3 DNA strand. The fluorescence signal appears to stabilize in all samples around 20 minutes. After 20 minutes the nanostars in the control that were still bound to 5pBT0Cy3, had about  $5.4 \times 10^6$  counts per 500 ms, while freed 5pBT0Cy3 had around  $4.7 \times 10^6$  counts per 500 ms. Nanostars bound to Cy3 had approximately 1.15 times more signal compared to the freed Cy3-biotin-linker. This provided sufficient evidence to support our hypothesis that the Cy3 DNA strands were actually attached to the gold nanostars inducing the metal enhanced fluorescence.

## REFERENCES

- 1 J. D. Ramsey, L. Zhou, C. K. Almlie, J. D. Lange and S. M. Burrows, *New J. Chem.*, 2015.
- 2 P. Dey, W. Olds, I. Blakey, K. J. Thurecht, E. L. Izake and P. M. Fredericks, *J. Raman Spectrosc.*, 2013, **44**, 1659–1665.
- 3 C. G. Khoury and T. Vo-Dinh, *J. Phys. Chem. C*, 2008, **112**, 18849–18859.
- 4 J. Lakowicz, M. Chowdhury, K. Ray, J. Zhang, Y. Fu, R. Badugu, C. Sabanayagam, K. Nowaczyk, H. Szmecinski, K. Aslan, and C. Geddes. *NCBI. PMID*. 2006.
- 5 L. Zhou, Ramsey, Jacob D., C. Kyle Almlie and Burrows, Sean M., *Manuscr. Prep.*, 2016.
- 6 J. R. Lakowicz, *Anal. Biochem.*, 2005, **337**, 171–194.

Chapter 3  
Building a Raman Instrument

## INTRODUCTION

Fluorescence spectroscopy is commonplace in analytical labs around the world. Studies commonly show limits of detection at the femto-micromolar levels. However, the broad excitation and emission profiles, typically over 100 nm, limits the capabilities and advantages of fluorescence. In particular, analysis in complex matrices or when analyzing multiple fluorescent species becomes challenging. An alternative technique known as Raman spectroscopy provides analytical signals that are typically only a few nanometers or less in breadth. Unfortunately, Raman scattering is a low probability event, and results in a very weak signal, not applicable in many cases.<sup>1</sup>

Raman scattering is a vibrational spectroscopy similar to IR. IR vibrational modes result from changes in the polarization of a bond whereas Raman vibrational modes result from changes in the polarizability of bond. Raman scattering occurs when a Raman active vibrational mode absorbs a photon and excites an electron to a virtual energy level.<sup>1</sup> This electron then drops down to a lower energy level and scatters a photon as a part of the radiative decay. The electron does not, however, return all the way to the ground state. Because of this, the scattered photon is actually a lower wavelength than the incident photon. This type of Raman scatter is referred to as Stokes scatter, and it gives important vibrational information about the molecule.<sup>1</sup> Raman spectra result from specific vibrational modes, so every Raman active molecule has a distinct Raman spectrum. This spectrum is inherently weak due to a low probability that is inversely proportional to the frequency of light to the fourth power. Roughly, only one in every 10 million photons results in a Raman scattering event.<sup>1</sup> Using a metal surface in proper proximity to a Raman dye can induce the Surface Enhanced Raman Scattering (SERS) effect. SERS can achieve signals as bright as fluorescence, while maintaining the narrow spectral profiles characteristic of Raman vibrational modes.<sup>2</sup>

To take advantage of the SERS technique a new Raman instrument was built. In the past, the Burrows lab had a functioning Raman system that was capable of detecting SERS signals. However, it was no longer functioning at the time of these studies. Using knowledge and lessons gained from working with the previous system, I built a new Raman instrument to be used in our work designing SERS based

biosensors. This chapter will detail the development of the Raman instrument I designed and built. Chapter 4 includes some of the initial data acquired and studies performed using the new instrument. Prior to building the instrument, certain aspects of our future biosensors needed to be considered.

SERS is a valuable technique that takes advantage of local surface plasmons on metal nanoparticles or nano-roughened surfaces. For our optimal SERS signal, the nanostar sample must be excited just red of the nanoparticle's/nanosurface's maximum plasmon resonance frequency.<sup>3</sup> In other words, it must be excited at a wavelength just longer than the  $\lambda_{\text{max}}$ . This is essential to maximizing the photonic interaction and therefore the signal enhancement. Exciting red of the plasmon  $\lambda_{\text{max}}$  significantly decreases self-absorption of Raman scattered light by the nanostars.<sup>2</sup> Different nanoparticles have differing optimal frequencies for excitation. For example, silver nanoparticles have plasmon maximums near 400 nm and gold nanospheres have plasmon maximums near 500 nm.<sup>4</sup> Thus, multiple excitation wavelengths are necessary to allow the system to analyze multiple sample types, types of nanoparticles, and analytes. Access to multiple excitation wavelengths had a strong influence in the design of the system in an effort to make it as versatile as possible.

## **DISCUSSION**

The Raman instrument was designed to include multiple lasers for access to multiple excitation wavelengths. The optical train is shown below in Figure 3-1. The system was designed to have two fiber optic locations: one for visible light and one for near infrared light. Due to the presence of both visible and near infrared lasers (NIR), it was inefficient to position these all on the same train as there are no lenses that can correct for the different focal lengths caused by chromatic aberrations of both visible and NIR light. If we tried to use the 785 nm laser on the visible collection fiber optic, the light would not focus to the proper location. This would significantly affect the collection efficiency of the system. To maximize the collection efficiency, two branches were designed: one branch for the visible light (532 nm and 633 nm) and one for the NIR 785 nm light. The visible branch utilizes all achromatic lenses to correct for chromatic aberration over the visible spectrum.

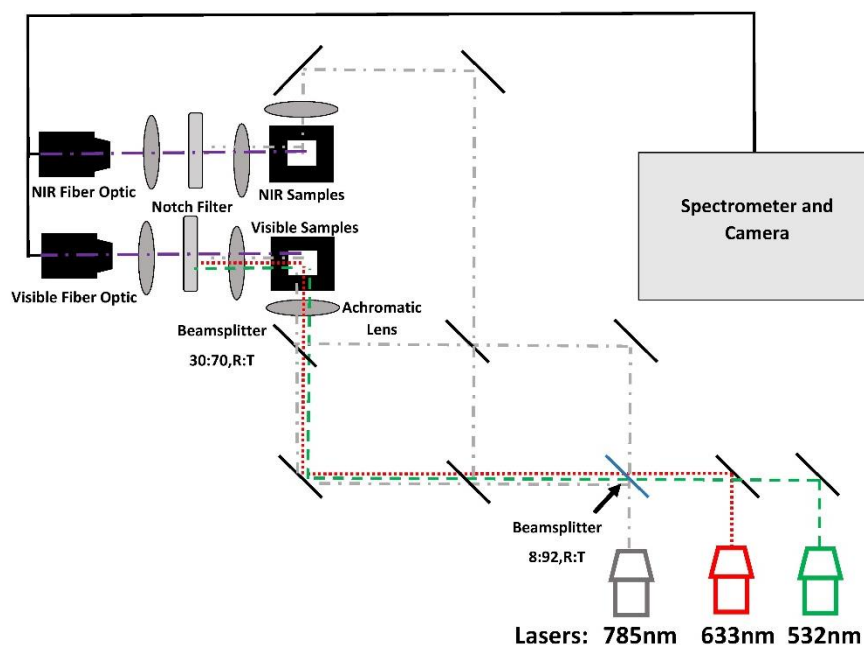


**Figure 3-1.** The designed Raman system has multiple mirrors on flip mounts giving the system access to three excitation wavelengths (532, 633, and 785 nm). The 785 nm laser has a pellicle mirror that reflects 8% of light and transmits 92%. The system is designed to have access to both of these laser powers. There is room for additional lasers to be added in the future.

The 785 nm light is initially separated into two beams: one beam is 92% of the original power and the other is 8% of the original power. It is possible to direct the more powerful portion of the 785 nm beam to the visible sample station using a beam splitter. This technique will be used in the future to excite nanostars at both visible and NIR wavelengths simultaneously in an effort to further enhance signals. Otherwise, either the 92% power portion of the beam or the less powerful 8% portion can be directed to the NIR sample station. The access to excitation at various powers and the incorporation of various excitation wavelengths makes the design of our instrument very versatile and capable of working with a variety of nanoparticles and systems.

## REFERENCES

- 1 D. Skoog, J. Holler and S. Crouch, *Principles of Instrumental Analysis*, Cengage Learning, 2006.
- 2 H. Yuan, Y. Liu, A. M. Fales, Y. L. Li, J. Liu and T. Vo-Dinh, *Anal. Chem.*, 2013, **85**, 208–212.
- 3 H. Yuan, A. M. Fales, C. G. Khoury, J. Liu and T. Vo-Dinh, *J. Raman Spectrosc.*, 2013, **44**, 234–239.
- 4 A. M. Fales, H. Yuan and T. Vo-Dinh, *J. Phys. Chem. C*, 2014, **118**, 3708–3715.

## Chapter 4

# Experiments in Surface Enhanced Raman Scattering: Using Plasmons to Enhance Signals

## INTRODUCTION

MicroRNA are small, non-coding RNA that act to disrupt protein translation and target proteins for degradation. Disease associated changes in microRNA are gaining interest as researchers learn about the underlying mechanisms of disease. Furthermore, these biomolecules are of interest as diagnostic and therapeutic targets.<sup>1</sup>

The Burrows lab is interested in creating innovative new biosensors to detect microRNA combinations called “Molecular Logic Sensors.” Each of these sensors has the potential to detect the presence of multiple microRNA’s. Since there are many multiple combinations of different microRNAs, many types of Molecular Logic Sensors will need to be made. This is where multiplexing capabilities become very valuable. Due to the narrow spectral profiles of Raman bands, we expect to be able to detect anywhere from 3-5 different Raman dyes. If each sensor can detect 3 microRNA as inputs, then this means we can detect 9-15 different combinations of microRNA simultaneously. If each Logic Sensor gives information about the microRNA’s present, then multiple sensors yield increased information, clarity, and insight into disease stages and progression. This ultimately leads to an enhanced level of characterization.

Fluorescence spectroscopy is one of the prevailing methods for designing biosensors for detecting these microRNA’s, but these capabilities can be somewhat limited.<sup>1</sup> Broad peaks reduce the multiplexing capabilities and can limit possible detection schemes. The use of more than 1 or 2 dyes would be difficult due to the broad spectral peaks of fluorescent bands. On the other hand, SERS has very narrow peaks, typically less than a few nanometers, which allows for multiplexing with very limited interference between different species in solution. Enhanced multiplexing capabilities with femtomolar limits of detection have been reported.<sup>2,3</sup>

SERS technologies do have some issues associated with reproducibility.<sup>4</sup> SERS utilizes sharp angled metals or rough nanosurfaces to create plasmonic hotspots that interact with dyes to create enhanced photonic interactions and signals. The reproducibility of the signal is strongly influenced by these nanosurfaces. If the surface is not reproducible, then it is difficult to obtain a reproducible signal.<sup>3</sup> The purpose of Chapter 1 was to develop a procedure to overcome issues with plasmon reproducibility. Our work with gold nanostar synthesis has led to increased reproducibility of signals

and certain aspects of nanostar morphology.<sup>5</sup> While the reproducible surface substrate is important, creating reproducible hotspots presents its own unique set of challenges. SERS, in aqueous solution, is highly dependent on the characteristics of the colloid. Some of these characteristics, such as aggregation of the colloid, were studied in detail in Chapter 1. This aggregation state has been shown to have a critical influence on the SERS signal enhancement.<sup>4</sup> The ionic strength and pH of the solution can also have a strong influence on the colloidal stability. Maintaining a stable colloid can be a challenge but is essential to solution based SERS.

In Chapter 1 we showed a technique for increased reproducibility and control over plasmon bands and certain aspects of the morphology of gold nanostars. While these intrinsic properties were shown to be more reproducible, we have yet to confirm the influence of this increased reproducibility of plasmon bands and morphology on SERS signals. This will be the subject of future studies. This chapter will detail some of the studies performed in an attempt to optimize the solution conditions of the gold nanostars to optimize enhancement. We work on both single nanoparticle and multi-nanoparticle SERS. In Chapter 4 I demonstrate the ability to obtain basic Raman signals and multiplex analysis, show work with silver nanoparticles as a basis for understanding how solution conditions can influence the SERS signal, describe SERS signal as a function of gold nanostar concentration, characterize the sensitivity of the developed Raman instrument, and demonstrate SERS with coupled gold nanostars (creating SERS hotspots between two particles).

## **EXPERIMENTAL**

All nanostars were synthesized using the procedures developed in Chapter 1. A 10 mW, 633 nm HeNe laser was used to excite the plasmon for all studies. Solutions were made to be 5 mM KCl by diluting to proper GNS concentration with a KCl solution.

### ***pH Influence on Silver Nanoparticle SERS Enhancement***

Approximately 80 nm silver nanoparticles were coated with 2.5 microM pMBA. One sample was left in 5 mM KCl solution while the other was made to be pH 10.4 using KOH. Three samples were made with acquisition times of 30 seconds. This study used an Ocean Optics USB 2000 series spectrometer.

### ***GNS Concentration Study***

Gold Nanostars were coated by incubation in 2.5 microM pMBA (para-Mercaptobenzoic Acid) Raman dye overnight. Spectra were recorded at 1080  $\text{cm}^{-1}$  and 1590  $\text{cm}^{-1}$  and their intensity was evaluated in MatLab. A trapezoidal Riemann sum was utilized over the peak area to obtain an integrated peak intensity. Three exposures of 20 seconds were averaged to create each frame, while 3 frames were averaged to obtain each spectra measured. Different concentrations of gold nanostars were obtained by diluting newly synthesized GNS so that the final solutions were 5 mM in KCl. This study utilizes dilutions of 0.00x, 0.05x, 0.10x, 0.15x, 0.20x, 0.25x, 0.30x, 0.45x, 0.60x, and 0.75x. A 2.5 microM pMBA in 5 mM KCl was used as the background. Spectra were acquired using an Acton SP2300 spectrometer (Holographic Grating, 1600 grooves/mm) and a Princeton Instrument EM-CCD camera.

### ***pMBA Calibration Curve***

Peak integration was utilized in this study with the same acquisition times and settings as the GNS Concentration Study. These values were recorded at 1590  $\text{cm}^{-1}$  and pMBA concentrations used were 5 nM, 10 nM, 100 nM, 250 nM, 400 nM, 600 nM, and 900 nM. Spectra were acquired using an Acton SP2300 spectrometer (Holographic Grating, 1600 grooves/mm) and a Princeton Instrument EM-CCD camera.

### ***GNS Coupling***

Gold Nanostars were coated with a biotinylated bovine Bovine Serum Albumin (BSA) for 2 hours at room temperature immediately post synthesis. Afterwards, they were separated into two different samples and one was coated in avidin and left to incubate for 2 hours at room temperature while the other sample was left unchanged. After 2 hours, the two solutions were combined and incubated overnight in order to promote the binding of biotin from the avidin-free nanostars to the avidin on the other stars. Some moderate signs of aggregation were seen in the morning indicating that

the nanostars had begun to couple together. The solution was sonicated briefly to disperse the nanostars. Spectra were recorded in the same manner discussed above. Spectra were acquired using an Acton SP2300 spectrometer (Holographic Grating, 1600 grooves/mm) and a Princeton Instrument EM-CCD camera.

## **RESULTS AND DISCUSSION**

### ***Proof of Raman Detection and Multiplexing***

After development of the Raman Instrument it was necessary to demonstrate the capability to obtain simple Raman spectra of common molecules. Ethanol (99%) and Toluene were utilized in this proof of concept experiment. This opportunity was also used to demonstrate the multiplexing capabilities mentioned throughout this work. Figure 4-1 shows the Raman spectra of ethanol, toluene, and a mixture of the two. The peaks are narrow and are mostly distinguishable from one another. Even in a solution that is just 1% Toluene and 99% Ethanol (99%) the peaks are well defined for Toluene amongst the Ethanol peaks. This ability to distinguish multiple species in a single solution can be applied to multiple Raman dyes in a solution allowing you to run multiple assays simultaneously.

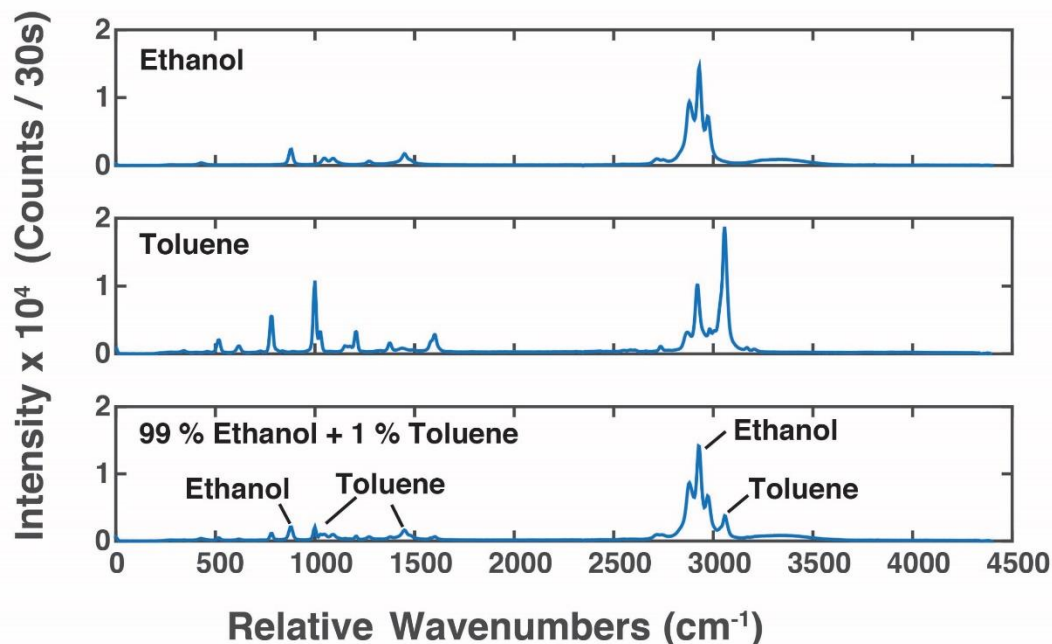


**Figure 4-1.** This figure presents the Raman spectra of ethanol, toluene, and a mixture of the two. The mixture clearly show the ability to obtain multiplexing measurements using Raman spectroscopy. An Ocean Optics USB 2000 series spectrometer was used to collect this data.

### ***pH Influence on Silver Nanoparticle SERS Enhancement***

Ionic strength of the solution and pH both play a critical role in how a colloid is able to perform in solution based SERS. Ionic strength is known to affect the aggregation state of the gold nanostars which plays a critical role in the Raman signal. There is an optimal level of aggregation to induce the most powerful signal enhancement. Previous work with silver nanoparticles and gold nanostars showed stability in a 5 mM KCl solution. We have shown that the 5 mM concentration induces minimal aggregation and in most cases resulted in a slight enhancement of the SERS signal (data not shown). When the nanostars are no longer in a colloidal suspension, they are unable to produce a SERS signal.

In this study we looked at the effect of pH on the SERS signal intensity. A search of literature indicated that a basic pH of around 10.4 would lead to an increased enhancement of prevalent Raman bands in pMBA. Figure 4-2 shows the SERS spectra of AgNP's with pMBA in a DI water matrix and a pH 10.4 matrix. The sample at pH 10.4 shows about a 100% increase in signal intensity over the pH neutral sample. It is

important to note that these results do not directly translate to our work with gold nanostars. Gold nanostars will likely require different pH conditions to achieve optimal signal enhancement. Silver nanoparticles and gold nanostars are different species and should be treated as such. However, this study does provide proof that altering certain qualities, such as pH, can have significant effects on the SERS signal of nanoparticles. Future work will investigate how the pH effects SERS in gold nanostars.

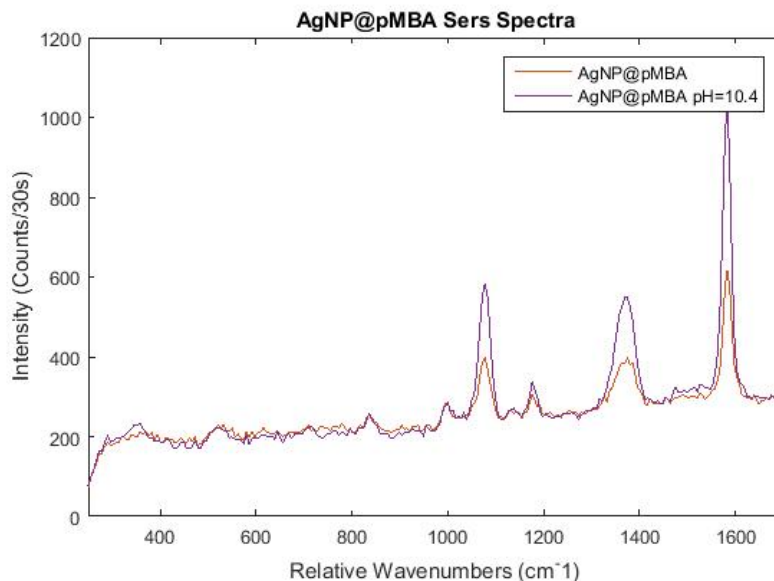


**Figure 4-2.** The SERS spectra of pMBA on silver nanoparticles. The sample at pH 10.4 shows a significant increase in signal over the pH neutral sample. Spectra is an average of 3 samples. Spectra have been background subtracted using pMBA in DI water as the background.

### ***GNS Concentration Study***

Initial studies were performed to characterize the SERS enhancements and optimal conditions for this spectroscopy. Care must be taken in evaluating the optical response of the nanoparticles and determining the optimal conditions to deliver the greatest signal enhancement. Nanoparticle concentration was explored in an effort to determine optimal concentration of GNS for signal enhancement.

The nanostar concentration contributes to the amount of light that is scattered, potential self-absorbance of Raman scattered light, and other factors that all contribute to signal intensity. S10 Gold Nanostars were synthesized according to the procedures developed in Chapter 1. The exact concentration of the nanostars synthesized was not known. Thus, this experiment refers to dilutions of the originally synthesized gold

nanostars. For example, .5x refers to a solution that was diluted in half. There was 500 microliters of gold nanostars solution with 500 microliters of DI water.

The signal enhancement was monitored under a constant dye concentration of 2.5 microM pMBA while varying the concentration used of the gold nanostars. The concentrations used were 0.00x, 0.05x, 0.10x, 0.15x, 0.20x, 0.25x, 0.30x, 0.45x, 0.60x, and 0.75x. Additionally, a 2.5 microM solution of just pMBA (no nanostars) was used as the background control. SERS was confirmed by comparison to the control.

The enhancement of each sample was calculated by subtracting the signal of the pMBA on the nanostars from the signal of the pMBA control in solution with no nanostars. In theory, we isolated the gold nanostar concentration as the only independent variable. Thus, any change in signal enhancement should be a direct result of the change in nanostar concentration. The change in signal enhancement is detailed in Figure 4-3.

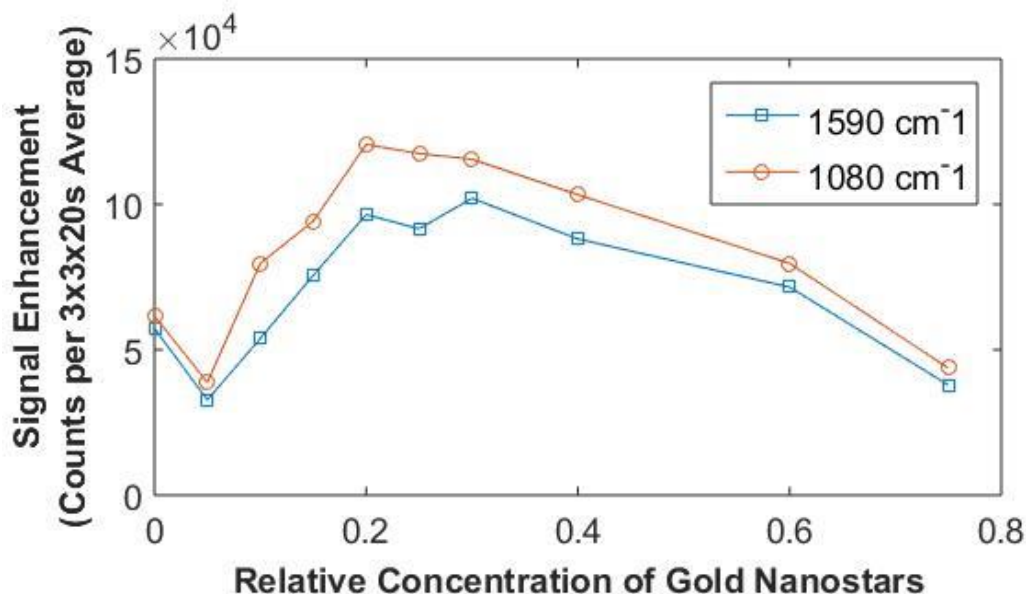


**Figure 4-3.** The signal enhancement as a function of gold nanostar concentration (with a constant pMBA Raman dye concentration of 2.5 microM). With an increasing nanostar concentration, the signal enhancement first increased, before it steadily decreased after a concentration of 0.30x nanostars.

The signal enhancement was monitored at two key positions where the pMBA dye has prominent signal enhancement. SERS was monitored at 1590  $\text{cm}^{-1}$  and 1080  $\text{cm}^{-1}$ . These values are relative to the laser line, which was 633 nm, and are not absolute

wavenumber values. The signal enhancement began to increase at both positions, 1590  $\text{cm}^{-1}$  and 1080  $\text{cm}^{-1}$ , with an increasing nanoparticle concentration. This increase occurred until the 0.20x-0.30x range. From this point, the signal enhancement over just the pMBA dye decreased steadily until 0.75x. This study allowed us to determine the optimal concentration for the gold nanostars when conducting SERS studies. We decided to proceed with a 0.25x value for nanostars to determine the SERS instruments' limit of detection for pMBA. It is important to note that this optimal concentration is likely only for the S10 nanostar species. Additional studies should be performed for other species such as S20 and S30 gold nanostars.

### ***pMBA Calibration Curve***

To evaluate the Raman instrument's sensitivity, the limit of detection for pMBA on gold nanostars was determined. The pMBA concentration was varied from 5 to 900 nM (5 nM, 10 nM, 100 nM, 250 nM, 400 nM, 600 nM, and 900 nM) in a 5 mM KCl solution. A 0.25x GNS concentration was used in these studies. The background samples were pMBA in 5 mM KCl solution. The Raman peak at 1580  $\text{cm}^{-1}$  relative to the 633 nm laser line was monitored in this study.

Figure 4-4 shows the increasing signal intensity as the concentration of pMBA was increased. This evaluation of the Raman instrument will provide a basis set of data to be used as a reference set in the future. For example, if the instrument is ever altered or improved, this study will be repeated for comparison to ensure we are improving the instrument's sensitivity (or at the very least, not decreasing the sensitivity). I expect to build an instrument with picomolar limits of detection or lower in the near future. Figure 4-4 showed a modest linear relationship, but concentration effects appear to be altering the relationship at 400 nM and above. Only one trial was performed, so further studies are needed to confirm a linear relationship, but these initial results show an inclination towards a linear relationship with a low nanomolar limit of detection.

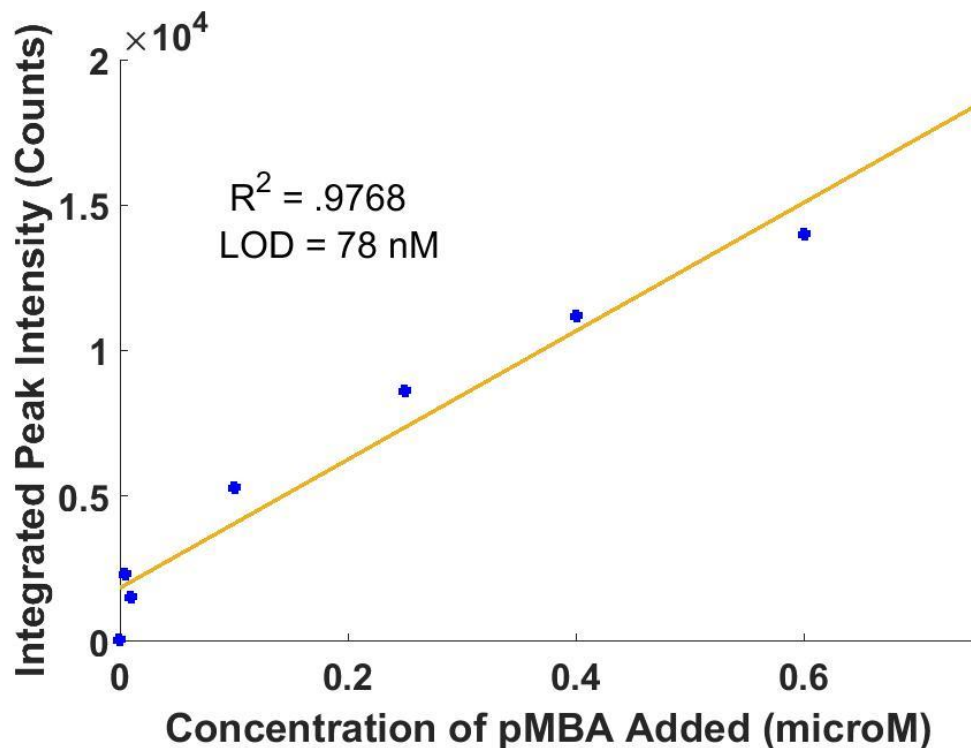


**Figure 4-4.** As the concentration of pMBA in the solution increased, the SERS signal intensity did as well. The limit of detection (LOD) was determined to be 78 nM.

#### *Coupling Gold Nanostars to Create SERS Hotspots*

The aggregation state of the gold nanostars plays a critical role in their signal enhancement. This is why the ionic strength and nanostar concentration were so heavily controlled and regulated. There exists an optimal colloidal state for obtaining a very intense signal enhancement. For example, when nanostars are coupled together, or kept in close proximity via various means, their plasmons can interact and lead to increased signal enhancement called a hot spot.<sup>4</sup> The BSA-Biotin-Avidin coupling experiment detailed below outlines my attempts to manipulate and control the nanoparticles by bringing them together in an attempt to obtain an even further increased signal.

Coupling of nanoparticles has been studied before and executed successfully in the past.<sup>4</sup> Their study coupled nanoparticles utilizing complimentary DNA base pairing. Our study utilizes a BSA-Biotin-Avidin pairing mechanism that is detailed in Figure 4-5. Initially, Nanostars were coated with Cy3 Raman dye. It is important to

note that Cy3 is a fluorescent molecule too, meaning this system could be utilized effectively in a Surface Enhanced Resonant Raman Scattering (SERRS) technique as well. SERRS utilizes excitation near an electronic level to increase signal enhancement by an order of magnitude.<sup>2</sup> However, in this experiment, we utilized a 10 mW 633 nm excitation beam that did not provide SERRS, but just SERS.

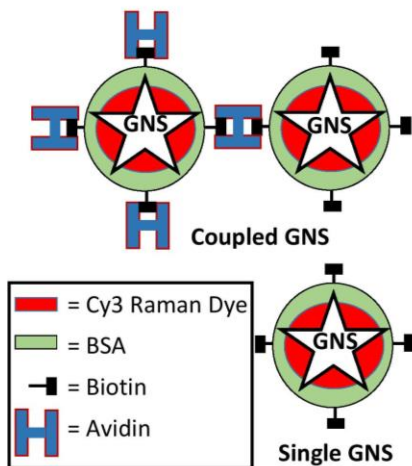


**Figure 4-5.** The mechanism for induced/controlled coupling in gold nanostars via BSA-Biotin-Avidin system. Nanostars are first coated in the Cy3 Raman dye and biotinylated-BSA before being coupled using biotin/avidin binding.

We hypothesized that by inducing coupling of the nanostars, the SERS signal would be more intense than SERS on single gold nanostars. We compared the coupled SERS with single nanostar SERS and just the Cy3 dye. As a control for no enhancement, free Cy3 dye was used. The single nanostars were coated in Cy3 and biotinylated-BSA, but no avidin was present. The coupled nanostars were coated with Cy3 and biotinylated-BSA, followed by addition of avidin to couple the nanostars.

Figure 4-6 shows the spectrum the three samples. Upon first glance, it looks as though there may be a slightly greater enhancement in the coupled nanostars relative to the single nanostars. However, the two enhancement levels were determined not to be significantly different ( $n=3$ ,  $p=0.05$ ). Just the Cy3 dye excited with the 633 nm laser showed a nearly flat signal with no indications of Raman activity. Thus, single nanostar SERS and coupled SERS both offer signal enhancement over just the Cy3 dye, but the preliminary data does not suggest a significant enhancement of coupled SERS over single gold nanostar SERS.

Further studies are needed to confirm these results. Perhaps the local environment needs to be different when performing coupled vs. single particle SERS. For examples, the charges on the surface of the nano-assembly could have prevented the biotinylated-BSA from interacting with the Avidin, Alternatively, the like charges on the biotinylated-BSA nanostars could have had repulsion that was stronger than the biotin-avidin interaction. Thus, further studies must be performed to determine optimal distance between particles, particle concentration, ionic strength, and pH for coupled SERS. With these studies, we may be able to produce a statistically significant enhancement of the Raman signal in coupled nanostars over single gold nanostar particles.

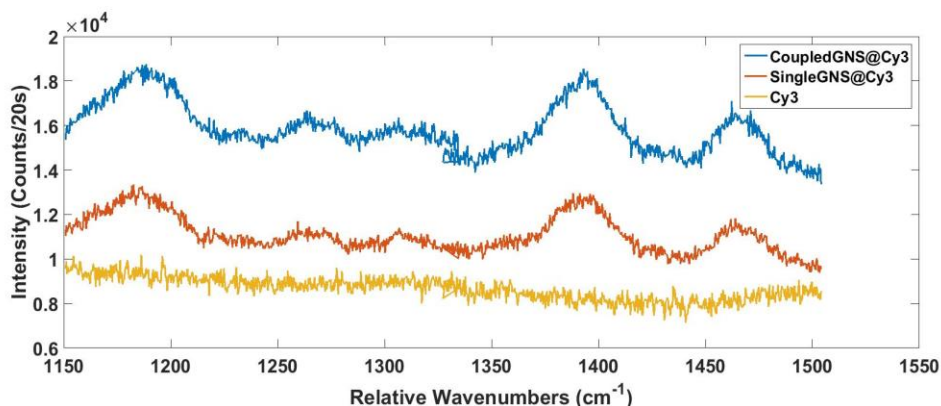


**Figure 4-6.** SERS signal from coupled Gold Nanostars, uncoupled Gold Nanostars, and Raman of just the Cy3 dye. Preliminary data suggests no significant difference in SERS signal between coupled and uncoupled GNS.

## CONCLUSIONS

Utilizing the novel synthesis technique developed in Chapter 1 of this Thesis, gold nanostars were synthesized with reproducible plasmon bands. After the Raman instrument was developed, the influence of nanoparticle concentration and nanoparticle coupling was evaluated. We also evaluated the sensitivity of the newly built Raman instrument. A relative concentration of .25x with a 5 mM KCl concentration was determined to be optimal for obtaining the greatest signal enhancement on the S10 nanostars. However, this could be different for each nanostar “species” meaning that further investigations are needed for other species (e.g. S20 and S30). A bio-conjugate

technique to control/induce nanostar coupling was investigated using a BSA-Biotin-Avidin system. Preliminary experiments indicated there was no significant enhancement over SERS with single gold nanostars. To evaluate our instrument, a simple calibration curve of pMBA on gold nanostars was collected. From the calibration curve a 78 nM limit of detection was determined for pMBA. Similar calibration curves will be used in the future for optimizing our instrument. The 78 nM pMBA benchmark will be used to ensure that future improvements made over time either meet or exceed that standard.

Preliminary studies have been completed in modifying our gold nanostars with DNA oligonucleotides. We were able to successfully obtain a SERS signal using a basic capture and reporter strand set up. Future work will design innovative new biosensors, like logic sensors, to interrogate dynamic and complex systems. With the narrow bands in the Raman spectra, and logic based sensors, we will be able to detect high numbers of microRNA's simultaneously. A disease cannot be diagnosed with just one marker, so the ability to obtain information on mircoRNA expression profiles across the board will provide a valuable diagnostic tool to learn about microRNA biology and for diagnosing diseases and disease states.

## REFERENCES

- 1 R. M. Graybill and R. C. Bailey, *Anal. Chem.*, 2016, **88**, 431–450.
- 2 H. Yuan, Y. Liu, A. M. Fales, Y. L. Li, J. Liu and T. Vo-Dinh, *Anal. Chem.*, 2013, **85**, 208–212.
- 3 H. Yuan, A. M. Fales, C. G. Khoury, J. Liu and T. Vo-Dinh, *J. Raman Spectrosc.*, 2013, **44**, 234–239.
- 4 H.-N. Wang and T. Vo-Dinh, *Small*, 2011, **7**, 3067–3074.
- 5 J. D. Ramsey, L. Zhou, C. K. Almlie, J. D. Lange and S. M. Burrows, *New J. Chem.*, 2015.

## **Acknowledgements**

*Conflict of Interest:* The author declares no competing financial interest.

The authors acknowledge Oregon State University for support of this research. Especially from the Research Office General Research Grant.

(The Oregon State University Electron Microscopy Suite)

The electron microscopy facility used to acquire TEM images is supported by the National Science Foundation via the Major Research Instrumentation (MRI) Program under Grant No. 1040588. We also gratefully acknowledge financial support for the acquisition of the TEM instrument from the Murdock Charitable Trust and the Oregon Nanoscience and Microtechnologies Institute (ONAMI).

We would like to thank and extend our great appreciation to the Koley Group (Oregon State University) for the use of their UV/Vis spectrophotometer. In addition, we would like to thank the Harper Group (Oregon State University) for the use of their Nanosight instrument.

## *Funding Sources*

We would like to thank Oregon State University and the Research Office General Research Grant for supporting this work. C. Kyle Almlie would like to thank the Milton Harris Graduate Fellowship for summer support toward this project. Jacob Ramsey would like to thank the Summer Undergraduate Research Experience (SURE) grant from the College of Science at Oregon State University for supporting this work.